Elucidating the dynamics of Integrin αIIbβ3 from native platelet membranes by cryo-EM with build and retrieve method

Xu Han, Zhemin Zhang, Chih-Chia Su, Meinan Lyu, Masaru Miyagi, Edward Yu, Marvin T. Nieman

Case Western Reserve University, School of Medicine, Cleveland, OH 44106;

Running title: Integrin αIIbβ3 structures from human platelets

Correspondence: Marvin T. Nieman
Department of Pharmacology
Case Western Reserve University
2109 Adelbert Road W309B
Cleveland, OH, 44106-4965
USA
Tel: +1 216 368 0250
E-mail: marvin.nieman@case.edu

Xu Han
Department of Pharmacology
Case Western Reserve University
2109 Adelbert Road W309B
Cleveland, OH, 44106-4965
USA
E-mail: xxh112@case.edu

Word court for text: 4052
Word count for abstract: 248
Figure count: 7
Table count: 3
Supplemental figure count: 5
Reference count: 38

Scientific category:

Key points:

- We report the first structural analysis of platelet membrane proteins extracted directly from human platelet membranes.
- Our novel structural-omics approach allowed us to solve integrin αIIbβ3 structures in two distinct states from resting human platelets.
- Regulatory cues of integrin αIIbβ3 were preserved from the native resource and revealed on the models with atomic resolutions.
- This study opens the potential to build the platelet membrane protein atlas to understand platelet physiology.

Abstract:

Platelets fulfill their essential physiological roles sensing the extracellular environment through their membrane proteins. The native membrane environment provides essential regulatory cues that impact the protein structure and mechanism of action. Single-particle cryogenic electron microscopy (cryo-EM) has transformed structural biology by allowing high-resolution structures of membrane proteins to be solved from homogeneous samples. Our recent breakthroughs in data processing now make it feasible to obtain atomic-level-resolution protein structures from crude preparations in their native environments by integrating cryo-EM with the "Build-and-Retrieve" (BaR) data processing methodology. We applied this iterative bottom-up methodology on resting human platelet membranes for an in-depth systems biology approach to uncover how lipids, metal binding, post-translational modifications, and co-factor associations in the native environment regulate platelet function at the molecular level. Here, we report using cryo-EM followed by the BaR method to solve the first unmodified integrin αIIbβ3 structure directly from resting human platelet membranes in its inactivated and intermediate states at 2.75Å and 2.67Å, respectively. Further, we also solved a novel dimer conformation of αIIbβ3 at 2.85Å formed by two intermediate-states of αIIbβ3. This may indicate a previously unknown self-regulatory mechanism of αIIbβ3 in its native environment.

In conclusion, our data show the power of using cryo-EM with the BaR method to determine three distinct structures including a novel dimer directly from natural sources. This approach allows us to identify unrecognized regulation mechanisms for proteins without artifacts due to purification processes. These data have the potential to enrich our understanding of platelet signaling circuitry.

Introduction

Platelets are central players in primary hemostasis, thrombosis, inflammation, and vascular biology.[1,2] Additionally, platelets have critical roles in diverse physiological and pathological processes ranging from inflammation and host defense to cancer, neurodegenerative, and cardiovascular diseases.[3-5] Platelet membrane proteins serve as the first responders to environmental changes by relaying the extracellular information across the membrane to mediate the platelet response.[5-7] While platelets patrol the integrity of the vascular system, membrane proteins sense and are regulated by their microenvironment. Establishing the interaction network of platelet membrane proteins will further our understanding of platelet responses.

Structural biology approaches like crystallography and cryo-electron microscopy (cryo-EM) have uncovered the functions of platelet membrane proteins by obtaining high-resolution structures of G-protein coupled receptors, adhesion molecules, and other surface receptors.[8-10] They have also uncovered the binding sites and mechanisms of anti-platelet therapies. [11,12] However, to understand the impact of native environment, we need approaches beyond traditional structural biology. A combination of proteomics and high-resolution unmodified protein complex structures is essential to significantly advance our understanding of protein function *in situ*. Traditional proteomics offers valuable network insights but lacks high-resolution structural information. [13,14] Similarly, traditional structural approaches require highly purified homogenous protein samples, limiting their application in studying integrated systems within cells, tissues, or organs. [15] Moreover, the dynamics of membrane proteins pose further challenges to obtaining structural information without introducing stabilizing modifications in overexpression systems. [16-18] Finally, extensive purification of exogenously expressed proteins can lead to the loss of native regulatory cues and rare protein conformations.

Recent advancements in data processing now present the opportunity to bridge these gaps enabling us to gain unprecedented insights into the intricate workings of platelet membrane proteins in their native environment. These cutting-edge developments in the data processing algorithm make using cryo-EM to study whole-cell, tissue, or organ samples feasible.[19-23] A novel iterative methodology, Build-and-Retrieve (BaR), was developed to process heterogeneous cryo-EM sample datasets (**Figure 1**).[21] This methodology allows us to analyze crude samples by performing *in silico* purification during data processing from a large heterogeneous dataset. [19-23]

In this paper, we applied cryo-EM coupled with BaR to resting platelet membrane proteins at ~200 kDa from healthy individuals. We solved the structures of αIIbβ3 directly from native human platelet membranes. We identified αIIbβ3 structures in two distinct states, the inactivated and intermediate states, at 2.75 Å and 2.67 Å, respectively. We also observed a novel homodimer conformation at 2.85 Å in which the head regions of two αIIbβ3 molecules in intermediate states were facing each other.

Materials and methods

Cryo-EM sample preparation

Human platelet lysing, membrane protein extraction, and sample preparation for cryo-EM were performed as described previously. [20,21]The detailed protocols for the preparation of human platelets and cryo-EM samples are described in the **Supplemental Methods**.

Data collection and processing

A Titan Krios equipped with a K3 direct electron detector was used to collect data in super-resolution mode at 81,000 magnifications. Data were processed in the cryoSPARC V4.6.0 suite using the BaR protocol as described previously.[19-23] The detailed data processing strategies are described in the **Supplemental Figure 1**. Protein Identification, model building, and refinement were performed as described.[19-23] The detailed protocols for data collection, processing, model building and refinement are described in the **Supplemental Methods**.

Quantification and statistical analysis

Standard Gold Standard-Fourier Shell Correlation curves at a threshold of 0.143 were computed using cryoSPARC v4.6.0 to obtain the final resolutions of protein models. The final atomic models were evaluated using MolProbity.

Proteomic analysis of platelet membrane fractions

Sample preparation for proteomic analysis was performed as described previously. [20,21] The detailed protocols for protein digestion and identification are described in the **Supplemental Methods**.

Results

Using cryo-EM coupled with the "Build-and-Retrieve" (BaR) data processing methodology (**Figure 1**), we solved three distinct cryo-EM maps at resolutions of 2.75 Å, 2.67 Å, and 2.85 Å, respectively (**Table 1** and **Supplemental Figure 1**). After model building and protein identification, all three maps were integrin αIIbβ3 in three different states: inactivated bent state, intermediate extended state, and a novel homodimer state that was formed by two integrin molecules in the extended state. Although we did not target integrin αIIbβ3 specifically or intentionally, it was not surprising that integrin αIIbβ3 was the first identified protein as it is one of the most abundant membrane proteins on human platelets at ~200 kDa.[24]

We performed proteomic analysis to investigate the composition of the resting human platelet membrane peak at ~200 kDa and to verify the existence of integrin αIIbβ3 in the sample. Our analysis identified approximately 800 different proteins within the peak. **Table 2** shows the 35 most abundant proteins in the peak, ranked by iBAQ (intensity-Based Absolute Quantification) values, which are calculated by summing the intensities of all detected peptides of a protein and dividing this sum by the number of theoretically observable peptides for that protein. We confirmed the presence of integrin αIIbβ3 in the sample (**Figure 2, Table 3**). Unsurprisingly, the integrin β3 subunit was the second most abundant protein, followed by integrin αIIb as the third (**Table 2**).

Inactivated bent state of αIIbβ3 - The overall architecture

The cryo-EM structure of native inactivated αIIbβ3 adopts the bent conformation seen previously in the crystal structures of the ectodomain and the most recent cryo-EM model of full-length integrin in native lipids.[8,10] (**Figure 3, Supplemental Figure 2**) Our inactivated αIIbβ3 cryo-EM structure indicates that it is a heterodimer with overall dimensions of 114 Å x 82 Å x 110 Å, excluding the density of the nanodisc. The full topology of the heterodimer with all 12 extracellular subdomains of the ectodomain and the nanodisc density is clearly visible in the cryo-EM map, which makes assigning the molecule's orientation to the membrane surface feasible. However, no density is detected for the transmembrane α-helices and αIIb and β3 short cytoplasmic tails. Our αIIbβ3 structure is superimposable onto the X-ray structure of complete ectodomain of integrin αIIbβ3 (3FCS.pdb[25]) with an RMSD between the respective 1,521 Cαs of 2.033 Å, and to the two recent inactive αIIbβ3 cryo-EM structures (8T2V.pdb[8], and 8GCD.pdb[10]) with RMSDs between the respective 1,393 Cαs of 1.570 Å (8T2V.pdb) and 1308 Cαs of 1.141 Å (8GCD.pdb).[8,10] The overall architecture of our integrin structure agree with the previous structural observation,[8,10,26] indicating that solving high-resolution membrane protein structure directly from platelet membranes without purification using BaR data processing is feasible and valid.

The head and upper leg regions are 114 Å long measured from Thr150 (UniProt Entry: P08514 numbering) from the β-propeller domain to Thr501 at the end of the thigh domain; the lower leg region is 98.5 Å long measured from the calcium at the αIIb genu point to Glu991 at the end of the calf-2 domain. Although the TM α-helixes are not solved in the bent αIIbβ3 conformation, we can still assign the orientation of the ectodomain to the plane of the membrane since the nanodisc density is clearly visible. (**Figure 3**) The molecule forms an overall "squatting" conformation. (**Figure 3**) The β-propeller domain of the αIIb subunit forms a 36.4° angle to the thigh domain, and a 48.1° angle formed between the thigh and calf-1 domains. The calf-2 domain in the lower leg region forms a 62.5° angle to the cell

membrane. (**Figure 3, Supplemental Figure 2**) The head and upper leg regions of the β3 subunit (βI, hybrid, and PSI domains) form at a sharper 16.2° angle to the lower leg region (EGFs and β-tail domains), and the lower leg region forms a 36.1° angle to the cell membrane. (**Figure 3, Supplemental Figure 2**) The head and upper leg regions of αIIbβ3 form a plane that is tilted to the cell surface with a 49.2 ° angle, which leads to the more "relaxed" bending on the αIIb subunit and a tighter bending conformation on the β3 subunit. (**Figure 3, Supplemental Figure 2**) The molecule is 110 Å in height, measured from the highest point of the head region (His61 from the β-propeller domain) to the membrane surface. (**Figure 3, Supplemental Figure 2**)

Using the 3D Flexible Refinement (3DFlex) function embedded in the CryoSparc v4.6.0 suite[27,28], we determined the local motion and dynamics of the flexible αIIbβ3 from the cryo-EM dataset in the bent conformation. (**Supplemental Figure 2E**, and **Movie S1**) Even in the single high-resolution "canonical" 3D density map of αIIbβ3, the molecule displays conformational variability and flexible (nonrigid) motion: the lower leg region demonstrated the highest dynamics followed by the upper leg region. (**Supplemental Figure 2E**, and **Movie S1**) This flexibility leads to the molecule continuously oscillating on the cell membrane. In contrast, the entire head region is quite stable with minimal dynamics being observed. This is also in agreement with our local resolution map (**Supplemental Figure 2F**): the head region has the highest resolution (~2.5 Å) followed by the upper leg region (~3 Å). Due to the molecular flexibility, the resolution of the lower leg region ranges from 3.5 Å to +5 Å, where the β-tail has the lowest resolution.

Inactivated bent state of αIIbβ3 - Glycosylation and ion binding sites

As a glycoprotein, integrin αIIbβ3 has a total of eleven predicted N-linked glycans: five on the αIIb subunit (αIIb-N46 and αIIb-N280 in the β-propeller domain, αIIb-N601 in the thigh domain, αIIb-N711 in the calf-1 domain and αIIb-N962 in the calf-2 domain) (UniProt Entry: P08514 numbering); and six on the β3 subunit (β3-N346 in the βI domain, β3-N125 and β3-N397 in the hybrid domain, β3-N478 in the I-EGF1 domain, β3-N585 in the I-EGF3 domain and β3-N680 in the β-tail domain) (UniProt Entry: P05106 numbering). [29] Clear densities of all 11 N-glycans are visible in our cryo-EM map of integrin αIIbβ3, which was directly extracted from resting human platelet membranes without manipulation during sample enrichment (**Figure 4A**). In agreement with previous structural data,[30] we observed all ion binding sites on the molecule (**Figure 4B**). In other structural work that focused on purified αIIbβ3, additional Mg^{2+}, Ca^{2+}, or both were added to the buffer throughout the purification process. In contrast, we did not provide exogenous divalent ions to our heterogenous cryo-EM sample during our sample preparation except at the initial washing step of the intact platelet membrane with high salt buffer to remove soluble proteins. Therefore, all ion binding was straight from the original whole blood sample from the donors. There are four Ca^{2+} binding sites at the β-propeller domain, one Ca^{2+} at the αIIb genu point, and three divalent-ions at the βI-domain: a Ca^{2+} at the metal ion-dependent adhesion site (MIDAS), a Mg^{2+} at the adjacent to MIDAS (ADMIDAS), and a Ca^{2+} at the synergistic metal ion-binding site (SyMBS). (**Figure 4B**)

Inactivated bent state of αIIbβ3 - Liganded by an RGD-motif-containing peptide

Interestingly, the bent inactivated αIIbβ3 structure is liganded by a peptide that contains an Arg-Gly-Asp (RGD)-motif. (**Figure 4C**). In this "squatting" conformation, the fully accessible ligand binding site at the

heterodimer interface of αIIbβ3 is facing forward and is 62 Å from the membrane surface. The accessibility of the ligand binding site of αIIbβ3 in its bent conformation agrees with the two most recent αIIbβ3 cryo-EM structures.[8,10]

In our cryo-EM density map at 2.75 Å resolution, the ligand binding site of bent inactivated αIIbβ3 is occupied by a clear density of an RGD-motif-containing peptide. Our αIIbβ3 structure is superimposable onto the X-ray structure of integrin αIIbβ3 headpiece bound to fibrinogen γ chain peptide by Springer and colleagues[26] (2VDO.pdb) with an RMSD between the respective β-I domain 168 Cαs of 0.366 Å, an RMSD between the β-propeller domain 390 Cαs of 0.258 Å, and an RMSD between the entire headpiece 658 Cαs of 0.729 Å. In agreement with the previous work, the surface representation of the binding site shows that the RGD peptide sits on the grove formed between the heterodimer interface of αIIbβ3. Since our BaR sample of resting human platelet membrane was a direct extraction from the endogenous resource, and the RGD-motif is a conserved sequence recognized by the integrin binding site, this RGD-containing peptide should belong to a natural ligand of αIIbβ3. We were able to observe some peptide density extended from the RGD-motif. However, without knowing the precise amino acid sequence, we were unable to identify or track the origin of the peptide due to the weak electron density of the peptide.

Intermediate state of αIIbβ3 - The overall architecture

The highly dynamic nature of αIIbβ3 is required to fulfill its role in mediating inside-out and outside-in signaling. We also observed a second conformation of αIIbβ3 is the intermediate state in our BaR dataset from resting human platelet membrane. These structures indicate that the protein also displayed a flexible structural rearrangement on the inactivated platelet. Although the lower leg region was visible in the 2D classification (**Supplemental Figure 3B**), the electron density of the lower leg region was lost during the following data processing due to the highly dynamic nature of the protein. Only the closed headpiece, which contained the full head region and the upper leg region (β-propeller, Thigh, and partial Calf-1 domains on the αIIb subunit; and βI, Hybrid, PSI, and partial I-EGF1 domains on the β3 subunit) in the intermediate state of αIIbβ3 at 2.67 Å was solved. (**Figure 5A, Supplemental Figure 3**).

Comparison between intermediate and bent states of αIIbβ3

There is a distinct difference between the top views of the bent and intermediate states, which validated there were indeed two different conformations of integrin αIIbβ3 in our dataset. An additional density can be observed in the 2D projection of the top view of the bent conformation but not in the intermediate state. This density came from the lower leg region, which can be seen through the center of the headpiece from the top of the molecule. (**Supplemental Figure 4A**) On the other hand, the lower leg region extends outward and is no longer visible through the center of the headpiece in the intermediate state. (**Supplemental Figure 4A**) The RMSD between the respective 834 Cαs of the intermediate state and the same headpiece region in our inactivated bent state is 1.662Å, which indicates these two conformations are similar but not the same. Compared to the inactivated state, the most noticeable overall structural shift of the headpiece came from the thigh domain in the αIIb subunit (shifted 9 Å) and the hybrid (shifted 6 Å), PSI, and I-EGF1 domains (shifted 9 Å) in the β3 subunit. (**Supplemental Figure 4B**). In contrast to a clear electron density of an RGD-motif-containing peptide

in the bent conformation, the ligand-binding site of the intermediate state was unoccupied. The density of three divalent ions at the MIDAS, ADMIDAS, and SyMBS were equally strong in the bent conformation. (**Figure 4B**) However, the electron density of the Mg^{2+} at the ADMIDAS was significantly weaker than the other two Ca^{2+} in the intermediate state. (**Figure 5C**) This further supports the closed headpiece in the intermediate state is unliganded.

Seven glycosylation sites were elucidated within the solved region of the intermediate state: three on the αIIb subunit (αIIb-N46 and αIIb-N280 in the β-propeller domain and αIIb-N601 in the thigh domain); and four on the β3 subunit (β3-N346 in the βI domain, β3-N125 and β3-N397 in the hybrid domain, and β3-N478 in the I-EGF1 domain). This is similar to the inactivated state. (**Figure 5D**)

Novel homodimer of αIIbβ3 - The overall architecture and dimer interface

A novel homodimer conformation of αIIbβ3 at 2.85Å was also observed in which the head regions of two αIIbβ3 molecules in intermediate states were facing each other. (**Figure 6, top, Supplemental Figure 6**) This additional homodimer interface was formed between two αIIb subunits and locked two molecules in a "face-to-face" and "head-to-toe" conformation. (**Figure 6, bottom**) Specifically, there are two clusters of interaction formed between Ser60 - Gly62 on the β-propeller domain and Pro574 - Cys576 on the thigh domain, and another two clusters of interaction formed between Gly570 – His572 on the thigh domain and Asp460 on the β-propeller domain

The homodimer showed similar glycosylation and ion binding profiles compared to the previous two structures. Like the intermediate conformation, we did not observe any ligand density in either αIIbβ3 molecule of the homodimer. (**Figure 6, top**) Together with our observations in the first two structures, this unique integrin αIIbβ3 architecture identified directly from the native platelet membrane may indicate a previously unknown self-regulatory effect of αIIbβ3 to temporally regulate its ligand accessibility in the intermediate state.

Discussion

Platelets are essential for the vascular system's integrity and primary hemostasis. To keep the perfect balance between the quiescent inactivated state in normal conditions and quick activation upon injury, platelet function is orchestrated by a network of interactions between proteins and biomacromolecules on the membrane to sense and relay the extracellular stimulus across the membrane.[1,2,7] Mutations, structural modifications, or changes in expression levels of these proteins can profoundly affect platelet physiology and are associated with numerous disorders. [3,31] Further, the native membrane environment provides essential additional regulatory cues, such as ions, post-translational modifications, and endogenous ligands *in situ* that coordinate the protein structure and mechanism of action. Defining the physical interactions of this network of membrane proteins in the endogenous environment will shed light on understanding basic platelet biology and physiology.

Technological breakthroughs in single-particle cryo-EM enable solving near-atomic-resolution structures of macromolecules without high-quality crystals. This is critical for studying membrane proteins and larger complexes, as their sample preparation and crystallization are difficult. The rapid developments of cryo-EM expand the molecular weight range and allow protein structures to be solved directly from native cell extracts. However, solving multiple proteins or multiple states of a single protein from a raw heterogeneous sample remains a challenge for single-particle cryo-EM.

In this study we combined cryo-EM with the Build-and-Retrieve (BaR) data processing method to analyze the platelet membrane proteins to bridge structural biology with -omics. BaR is an iterative bottom-up approach that uses *in silico* purification to obtain high-resolution cryo-EM maps to solve structures of proteins in different states in the native environment.[19-23] Here, we report the unmodified integrin αIIbβ3 structure obtained directly from resting human platelet membranes in its inactivated and intermediate states at 2.75Å and 2.67Å, respectively. We also solved a novel homodimer conformation formed by two intermediate-states of αIIbβ3 at 2.85Å.

Integrin αIIbβ3, also known as GPIIb/IIIa, is a cell surface receptor that plays a crucial role in platelet function. When activated, αIIbβ3 undergoes conformational changes that enable it to bind to fibrinogen and other ligands, which further facilitates platelet aggregation. The previous structural studies with αIIbβ3 in different states have provided key insights on its mechanism of action. Our data with αIIbβ3 directly from resting human platelets add new information on the highly dynamic nature of this protein prior to activation. We also identified the structural rearrangement between the three states (**Figure 7**) and the local dynamics and flexibility of αIIbβ3 in the bent conformation.

Our αIIbβ3 structures in bent and intermediate conformations are in agreement with their corresponding crystal and cryo-EM structures. [8,10,25] Our cryo-EM sample was prepared directly from its native environment without additional affinity enrichment. This preserved the natural regulatory cues, such as glycosylation sites, ion binding, and co-factors, which new insights on how the environment regulates αIIbβ3 structure and function.

First, N-linked glycosylation is critical to regulating the adhesion function of integrins.[29] The role of each N-linked glycan on αIIbβ3 integrin structure and function was thoroughly studied by mutagenesis in

HEK293FT cells.[29] Our structural data provided additional clear visual support for the presence of all 11 N-linked glycans. (**Figure 4A**) Micro-, macro-, and meta-heterogeneity of glycosylation can impact protein structure and function.[32] We observed some level of micro- and macro-heterogeneity of N-linked glycosylation among the bent, intermediate, and dimer conformations. The structural and functional impact of heterogeneous glycosylation of integrin αIIbβ3 is an area for future exploration. The electron density was weaker in the I-EGF1 domain in both the intermediate and the dimer conformations. Thus, although we did observe a clear N-linked glycan around the N478 site in the β3 subunit, assigning the precise location of the NAG was challenging given that two additional asparagine residues (N475 and N509) were in close proximity. Future studies will determine the functional significance of the interplay of these three asparagines on N-linked glycosylation in the I-EGF1 domain.

Second, we observed all ion binding sites on the αIIbβ3 molecule. (**Figure 4B, 5B** and **5C**) Our goal is to solve structures of proteins from the human platelet membranes with minimal manipulation. We did not provide additional divalent ions during our sample preparation other than in the high salt buffer for removing soluble proteins from the intact platelet membrane at the initial step. To our surprise, there were clear electron densities of four Ca^{2+} binding sites at the β-propeller domain, one Ca^{2+} at the αIIb genu point, and three divalent-ions binding at the MIDAS, ADMIDAS, and SyMBS at the βI-domain, which indicated all ion binding was from the original whole blood from the donor. This demonstrates the power of our approach to preserve the interactions from the original native environment.

Third, the αIIbβ3 cryo-EM map of the bent conformation showed a clear density from a peptide that contains an RGD-motif at the ligand binding site. (**Figure 4C**) This agrees with the overall architecture of the bent conformation and the most recent cryo-EM structure of the full-length αIIbβ3,[8] in which the whole molecule was “squatting” on the lipidic nanodiscs and the ligand binding site was fully accessible. This could potentially challenge the conventional αIIbβ3 switchblade model on its activation mechanism, in which the headpiece of the molecule points to the membrane to maintain its low affinity for the ligand.[8] We cannot rule out that this observation may be due to the sample extraction strategy. Coller suggested that extraction conditions, by detergent only or by inserting into nanodiscs, affected the overall structure of αIIbβ3.[33] Therefore, further studies are needed to carefully evaluate the impact of the lipidic mimetic environment on αIIbβ3 structure.

We also identified a third conformation, which is a novel homodimer of αIIbβ3. (**Figure 6**) This new αIIbβ3 conformation highlights the strength of the BaR method in analyzing crude samples straight from their original sources with minimum manipulation in protein purification. Unlike other αIIbβ3 structural studies that used “traditional” approaches to purify the protein with affinity chromatography, we believe our minimum enrichment, with only size-exclusive chromatography, is the key to preserving this unique homodimer confirmation. Further, the additional homodimer interface formed by two αIIbβ3 molecules stabilizes the protein in its intermediate state before the full extension. Our working hypothesis is that homodimerization is a previously unknown self-regulatory mechanism to temporally regulate its ligand accessibility in the intermediate state. (**Figure 7**) Future studies are needed to validate this conformation in live cells and to determine its impact on αIIbβ3 function. However, we do currently have indirect evidence to support our hypothesis. Both extended αIIbβ3 molecules in the intermediate conformation and in the homodimer conformation were unliganded, which is distinct from the bent state.

(**Supplemental Figure 4**) Additionally, this homodimer conformation of αIIbβ3 may open a new avenue for antiplatelet therapy, suggesting a potential focus on the homodimer interface rather than directly targeting the ligand binding site of αIIbβ3.

Our results highlight the potential of cryo-EM coupled with BaR for system structural proteomics. BaR is an unbiased and untargeted approach. This method could be a double-sided sword that not only brings opportunities to simultaneously solve novel structures of proteins in different states from crude samples but also brings in inherent limitations. First, it is a challenge to solve the structure of a particular protein with low abundance in the crude sample. Second, the nature of the method makes it difficult to identify proteins with electron density maps lower than 4 Å resolution. Advances in cryo-EM sample preparation and the BaR methodology will overcome these limitations in future studies.

In conclusion, our study was the first to focus on platelets using a structural-omics approach that combines cryo-EM with Build-and-Retrieve data analysis. Using this approach, we were able to demonstrate the highly structural dynamics of αIIbβ3 from native platelet membranes, which actively rearrange among three different states: bent, intermediate, and homodimer. In addition, we showed the strength of the BaR methodology in preserving natural regulatory cues of the proteins from their environment. Our study highlights the potential of creating a structural atlas of platelet membrane protein complexes, which will ultimately enrich our understanding of the foundation of platelet signaling circuitry in response to surrounding, epigenetic, and genetic changes.

Acknowledgements:
MN receives research funding from the National Institutes of Health (NIH) and the National Heart Lung and Blood Institute (NHLBI) (HL098217 and HL154026). XH receives funding from the American Heart Association (AHA) Postdoctoral Fellowships (897185) and the American Society of Hematology (ASH) Fellow Scholar Award. This research was also supported in part by the grant AI145069 to EY from the National Institute of Allergy and Infectious Diseases (NIAID). We thank Belinda Willard and Ling Li at Lerner Research Institute's Proteomics & Metabolomics Core for the acquisition of mass spectrometry data. The timsTOF Pro2 mass spectrometer instrument was purchased via an NIH-shared instrument grant, S10 OD030398. We are grateful to the Cryo-Electron Microscopy Core at the CWRU School of Medicine and Drs. Kunpeng Li and Kyle Whiddon for access to the sample preparation and Cryo-EM instrumentation.

ORCiD:
Xu Han: 0000-0002-1977-1046
Zhemin Zhang: 0000-0003-0135-4970
Chih-Chia Su: 0000-0003-3646-327X
Meinan Lyu: 0000-0001-5795-0232
Masaru Miyagi: 0000-0003-4325-1216
Edward Yu: 0000-0001-5912-1227
Marvin Nieman: 0000-0003-2602-023X

Data availability
Coordinates and EM maps for three conformations of integrin αIIbβ3 can be found at PDB accession numbers 9E8A, 9E8B, 9E8C and EMDB accession codes EMD-40713, EMD-40715, EMD-40716, EMD-40686, EMD-40688, and EMD-40691, respectively. The MS proteomics data have been deposited to the ProteomeXchange Consortium (http://proteomecentral.proteomexchange.org) *via* the PRIDE partner repository with the data set identifier PXD058005.

Author Contribution:
XH, EY, and MN conceived the study. XH and MN designed the experiments. XH, CS, ZZ, ML, MM, and MN performed the experiments and analyzed the data. XH and MN wrote the manuscript. CS, ZZ, ML, MM, and EY critically read and edited the manuscript.

Conflict-of-interest statements:
The authors have no conflicts of interest to disclose.

References

1. Scridon A. Platelets and Their Role in Hemostasis and Thrombosis-From Physiology to Pathophysiology and Therapeutic Implications. *Int J Mol Sci*. 2022;23(21).

2. Tyagi T, Jain K, Gu SX, et al. A guide to molecular and functional investigations of platelets to bridge basic and clinical sciences. *Nature Cardiovascular Research*. 2022;1(3):223-237.

3. Melchinger H, Jain K, Tyagi T, Hwa J. Role of Platelet Mitochondria: Life in a Nucleus-Free Zone. *Front Cardiovasc Med*. 2019;6:153.

4. Smyth SS, McEver RP, Weyrich AS, et al. Platelet functions beyond hemostasis. *J Thromb Haemost*. 2009;7(11):1759-1766.

5. Cho SY, Hur M. Expanded Impacts of Platelet Functions: Beyond Hemostasis and Thrombosis. *Ann Lab Med*. 2019;39(4):343-344.

6. Hamilos M, Petousis S, Parthenakis F. Interaction between platelets and endothelium: from pathophysiology to new therapeutic options. *Cardiovasc Diagn Ther*. 2018;8(5):568-580.

7. Saboor M, Ayub Q, Ilyas S, Moinuddin. Platelet receptors; an instrumental of platelet physiology. *Pak J Med Sci*. 2013;29(3):891-896.

8. Adair BD, Xiong JP, Yeager M, Arnaout MA. Cryo-EM structures of full-length integrin alphaIIbbeta3 in native lipids. *Nat Commun*. 2023;14(1):4168.

9. Guo J, Zhou YL, Yang Y, et al. Structural basis of tethered agonism and G protein coupling of protease-activated receptors. *Cell Res*. 2024;34(10):725-734.

10. Huo T, Wu H, Moussa Z, Sen M, Dalton V, Wang Z. Full-length alphaIIbbeta3 cryo-EM structure reveals intact integrin initiate-activation intrinsic architecture. *Structure*. 2024;32(7):899-906 e893.

11. Zhang C, Srinivasan Y, Arlow DH, et al. High-resolution crystal structure of human protease-activated receptor 1. *Nature*. 2012;492(7429):387-392.

12. Nesic D, Zhang Y, Spasic A, et al. Cryo-Electron Microscopy Structure of the alphaIIbbeta3-Abciximab Complex. *Arterioscler Thromb Vasc Biol*. 2020;40(3):624-637.

13. Yugandhar K, Gupta S, Yu H. Inferring Protein-Protein Interaction Networks From Mass Spectrometry-Based Proteomic Approaches: A Mini-Review. *Comput Struct Biotechnol J*. 2019;17:805-811.

14. Amiri-Dashatan N, Koushki M, Abbaszadeh HA, Rostami-Nejad M, Rezaei-Tavirani M. Proteomics Applications in Health: Biomarker and Drug Discovery and Food Industry. *Iran J Pharm Res*. 2018;17(4):1523-1536.

15. Benjin X, Ling L. Developments, applications, and prospects of cryo-electron microscopy. *Protein Sci*. 2020;29(4):872-882.

16. Carpenter EP, Beis K, Cameron AD, Iwata S. Overcoming the challenges of membrane protein crystallography. *Curr Opin Struct Biol*. 2008;18(5):581-586.

17. Errasti-Murugarren E, Bartoccioni P, Palacin M. Membrane Protein Stabilization Strategies for Structural and Functional Studies. *Membranes (Basel)*. 2021;11(2).

18. Milic D, Veprintsev DB. Large-scale production and protein engineering of G protein-coupled receptors for structural studies. *Front Pharmacol*. 2015;6:66.

19. Lyu M, Su CC, Miyagi M, Yu EW. Simultaneous solving high-resolution structures of various enzymes from human kidney microsomes. *Life Sci Alliance*. 2023;6(2).

20. Morgan CE, Zhang Z, Miyagi M, Golczak M, Yu EW. Toward structural-omics of the bovine retinal pigment epithelium. *Cell Rep*. 2022;41(13):111876.

21. Su CC, Lyu M, Morgan CE, Bolla JR, Robinson CV, Yu EW. A 'Build and Retrieve' methodology to simultaneously solve cryo-EM structures of membrane proteins. *Nat Methods*. 2021;18(1):69-75.

22. Su CC, Lyu M, Zhang Z, et al. High-resolution structural-omics of human liver enzymes. *Cell Rep*. 2023;42(6):112609.

23. Tringides ML, Zhang Z, Morgan CE, Su CC, Yu EW. A cryo-electron microscopic approach to elucidate protein structures from human brain microsomes. *Life Sci Alliance*. 2023;6(2).

24. Burkhart JM, Vaudel M, Gambaryan S, et al. The first comprehensive and quantitative analysis of human platelet protein composition allows the comparative analysis of structural and functional pathways. *Blood*. 2012;120(15):e73-82.

25. Zhu J, Luo BH, Xiao T, Zhang C, Nishida N, Springer TA. Structure of a complete integrin ectodomain in a physiologic resting state and activation and deactivation by applied forces. *Mol Cell*. 2008;32(6):849-861.

26. Springer TA, Zhu J, Xiao T. Structural basis for distinctive recognition of fibrinogen gammaC peptide by the platelet integrin alphaIIbbeta3. *J Cell Biol*. 2008;182(4):791-800.

27. Punjani A, Fleet DJ. 3DFlex: determining structure and motion of flexible proteins from cryo-EM. *Nat Methods*. 2023;20(6):860-870.

28. Punjani A, Rubinstein JL, Fleet DJ, Brubaker MA. cryoSPARC: algorithms for rapid unsupervised cryo-EM structure determination. *Nat Methods*. 2017;14(3):290-296.

29. Cai X, Thinn AMM, Wang Z, Shan H, Zhu J. The importance of N-glycosylation on beta(3) integrin ligand binding and conformational regulation. *Sci Rep*. 2017;7(1):4656.

30. Adair BD, Xiong J-P, Yeager M, Arnaout MA. Cryo-EM structures of full-length integrin αIIbβ3 in native lipids. *Nature Communications*. 2023;14(1):4168.

31. Au AE, Josefsson EC. Regulation of platelet membrane protein shedding in health and disease. *Platelets*. 2017;28(4):342-353.

32. Caval T, Heck AJR, Reiding KR. Meta-heterogeneity: Evaluating and Describing the Diversity in Glycosylation Between Sites on the Same Glycoprotein. *Mol Cell Proteomics*. 2021;20:100010.

33. Coller BS. alphaIIbbeta3: structure and function. *J Thromb Haemost*. 2015;13 Suppl 1(Suppl 1):S17-25.

Figure Legends

Figure 1. Build-and-Retrieve (BaR) Pipeline. Integrating cryo-EM with the BaR data processing methodology allows us to obtain atomic-level-resolution protein structures directly from crude preparations straight from their native environment.

Figure 2. Peptide coverage of the human αIIbβ3 by MS. Full sequence of integrin αIIb (top) and β3 (bottom) were obtained from the UniProt database. The signal peptides were colored in red, and the mature proteins were colored in black. Each underline indicates a peptide of integrin αIIb (top) or β3 (bottom) identified from the mass spec study. Peptide coverage of integrin αIIb (top) and β3 (bottom) was highlighted in yellow.

Figure 3. The overall architecture of integrin αIIbβ3 in the bent conformation. A. The overall cryo-EM map of integrin αIIbβ3 in bent conformation at 2.75 Å resolution is shown. The integrin αIIbβ3 model was shown in ribbon diagrams with the αIIb subunit colored in royal blue and the β3 subunit colored in goldenrod here and in subsequent figures. **B.** A total 12 subdomains of the ectodomain are resolved. The integrin αIIbβ3 model was shown in ribbon diagrams with each subdomain colored as follows: β-propeller in purple, Thigh in lime green, Calf in light green, β-I in blue, Hybrid in salmon, PSI in green, I-EGFs in yellow, and β-tail in pink.

Figure 4. The interaction network of integrin αIIbβ3 in the bent conformation. A. 11-N-linked glycan sites were preserved in the bent integrin αIIbβ3 obtained from the native environment**. B.** Closeup of the cryo-EM density of the metal ions, one at the α-genu (top left insert), four at the β-propeller (top right insert), and three at SyMBS, MIDAS, and ADMIDAS of the β-I domain (bottom right insert). **C.** A clear density of an RGD-motif-containing peptide was observed in the ligand binding site.

Figure 5. The architecture of integrin αIIbβ3 in the intermediate conformation and its interaction network. A. The overall cryo-EM map of integrin αIIbβ3 in intermediate conformation at 2.67 Å resolution is shown. The right panel is the side of the headpiece facing the cell membrane. **B.** Closeup of the cryo-EM density of the four metal ions at the β-propeller domain. **C.** Closeup of the cryo-EM density of the three metal ions at SyMBS, MIDAS, and ADMIDAS of the β-I domain. D. 7-N-linked glycan sites within the solved region of the intermediate integrin αIIbβ3 were preserved**.**

Figure 6. A novel homodimer conformation formed by two intermediate integrin αIIbβ3 molecules was revealed. The overall cryo-EM map of integrin αIIbβ3 in homodimer conformation at 2.85 Å resolution is shown. The top right panel is the side of the headpiece facing the cell membrane. The bottom insert shows the closeup of the dimer interface formed by two αIIb subunits from two individual integrin αIIbβ3 molecules. The residues that are involved in the dimer interface were colored in red.

Figure 7. Proposed model for the dynamic of integrin αIIbβ3 on resting human platelet membrane. On the surface of the resting human platelets, integrin αIIbβ3 has three major conformations: inactivated bent, intermediate, and homodimer. An RGD-motif-containing ligand (red star) binds to the bent conformation and keeps the ligand binding site occupied when the molecule is

inactive. The ligand releases while αIIbβ3 extends to the intermediate state. Two adjacent αIIbβ3 molecules in the intermediate state can form a homodimer on the surface. There is a dynamical conformational equilibrium between the intermediate state and the homodimer state of αIIbβ3 on the human platelets.

Figure 1

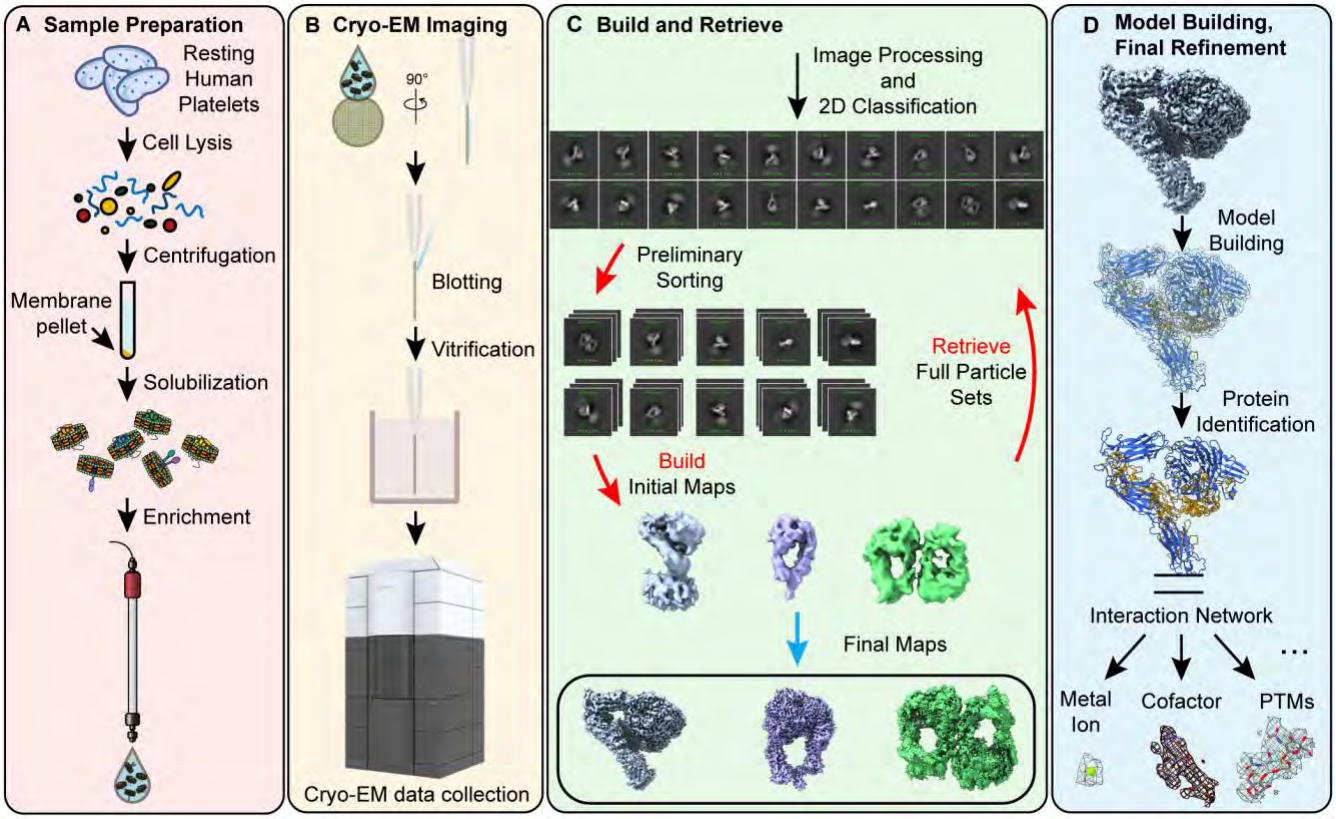

Figure 2

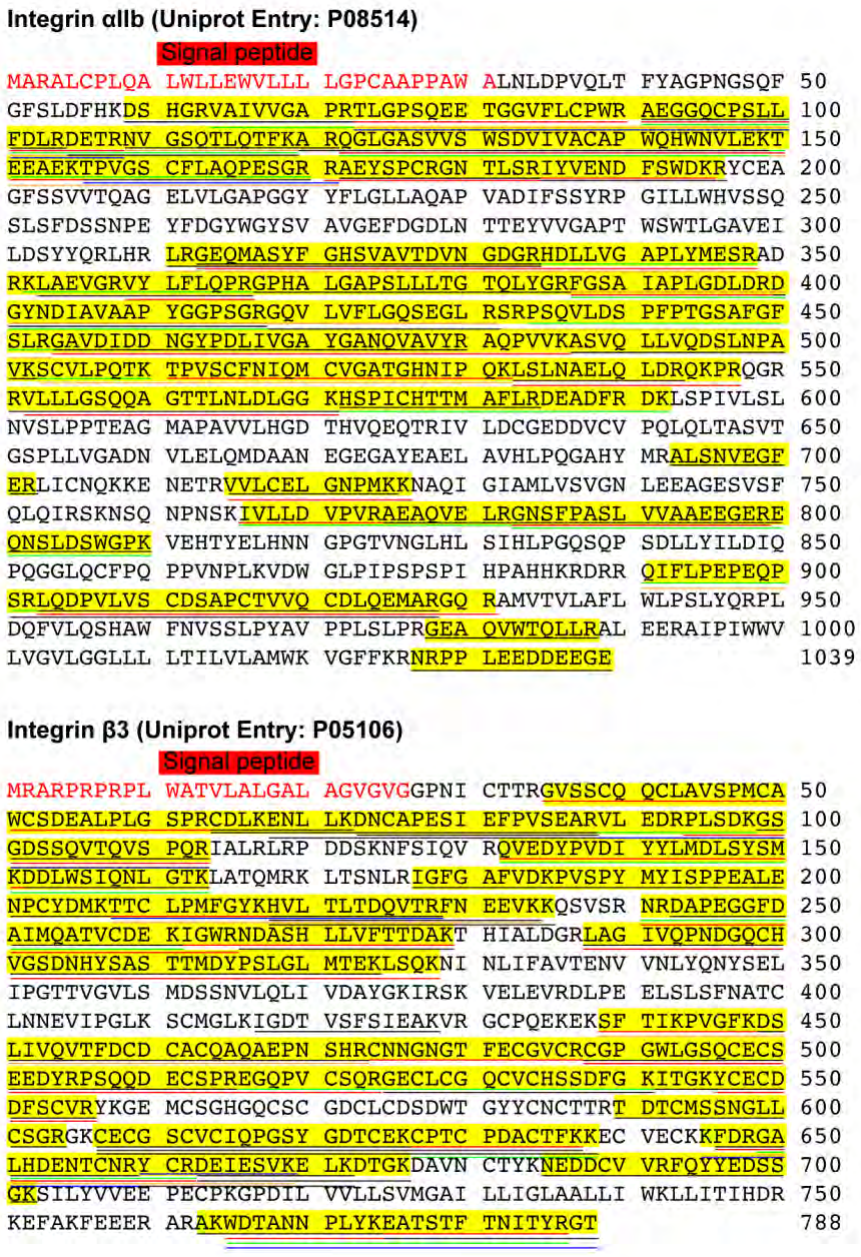

Figure 3

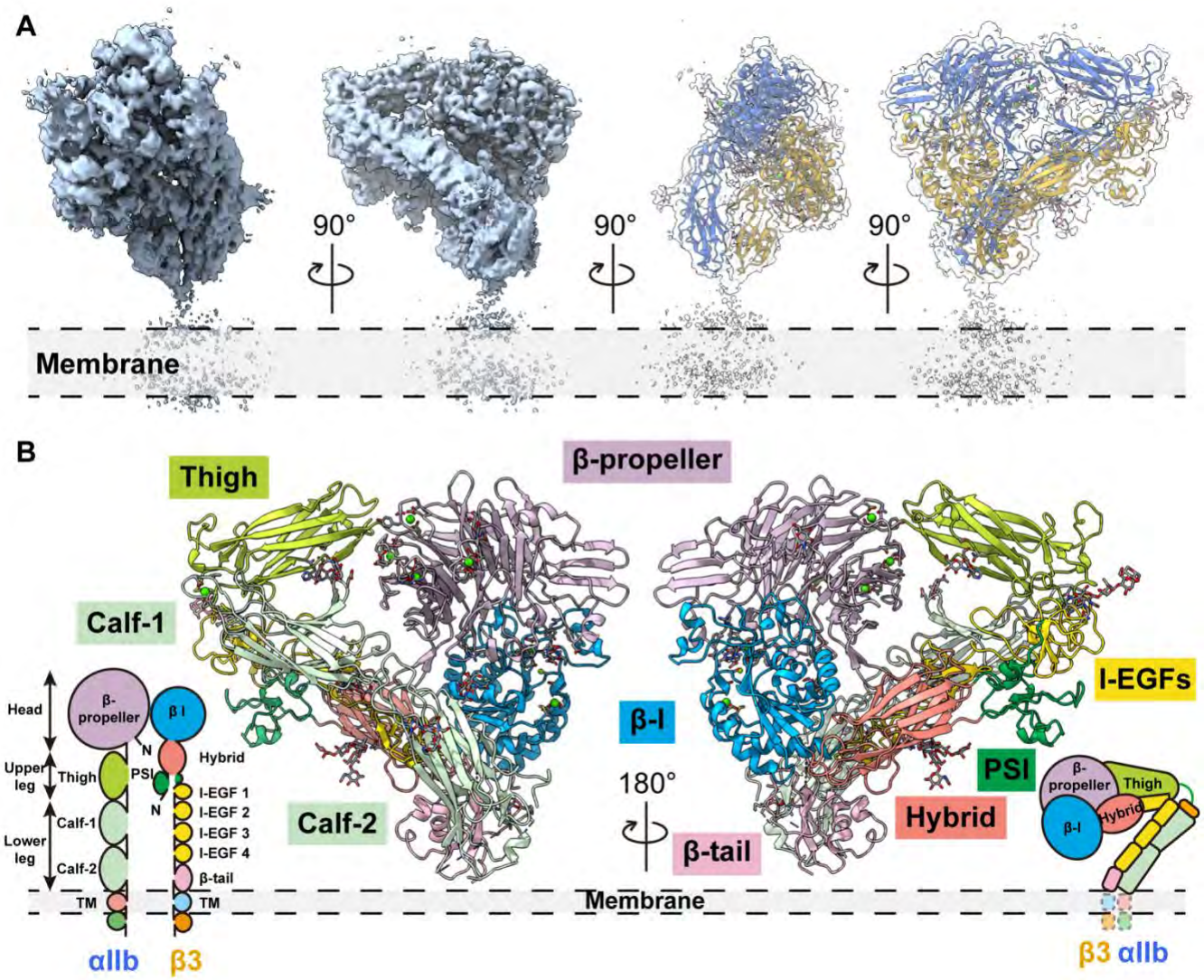

Figure 4

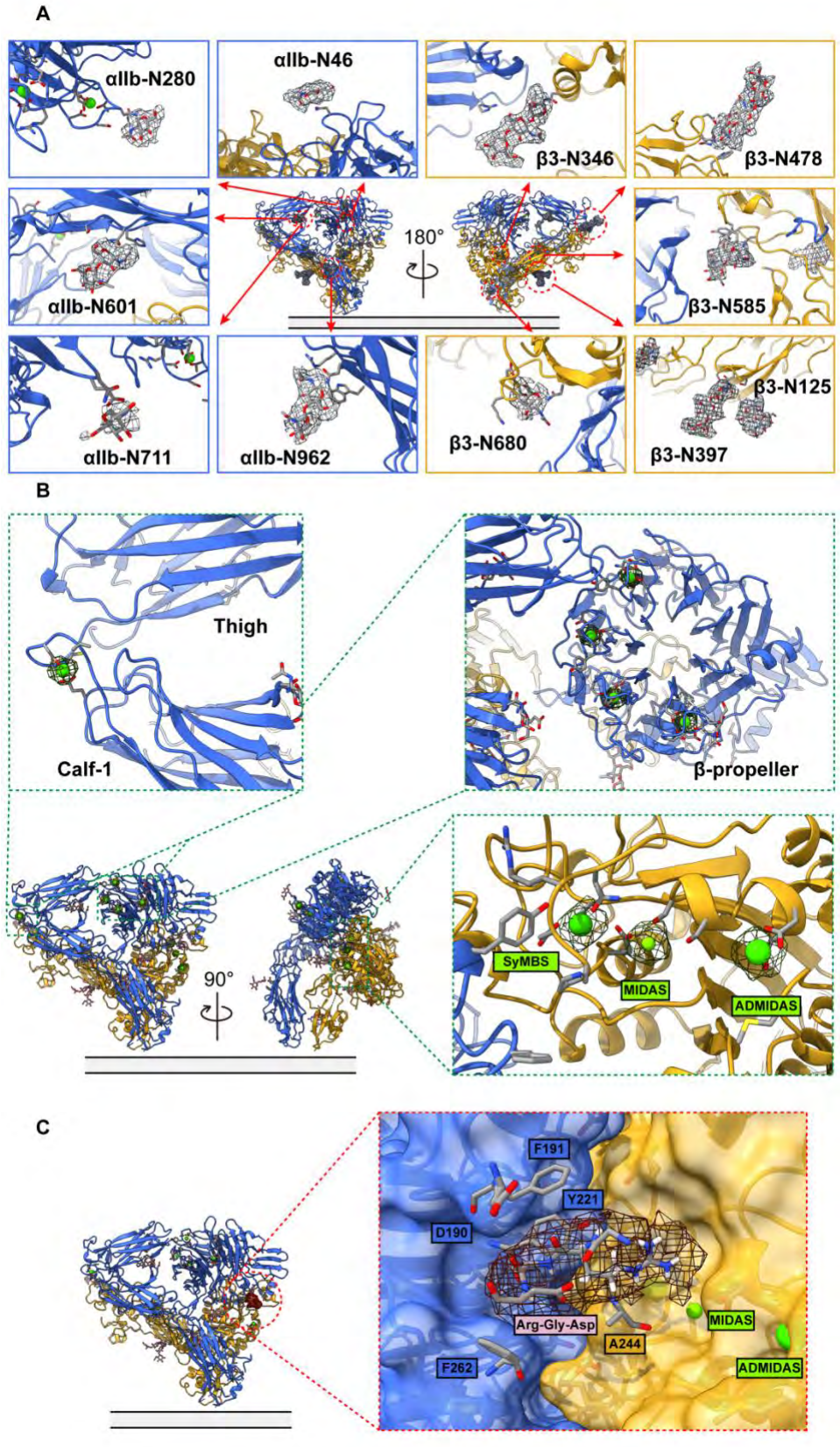

Figure 5

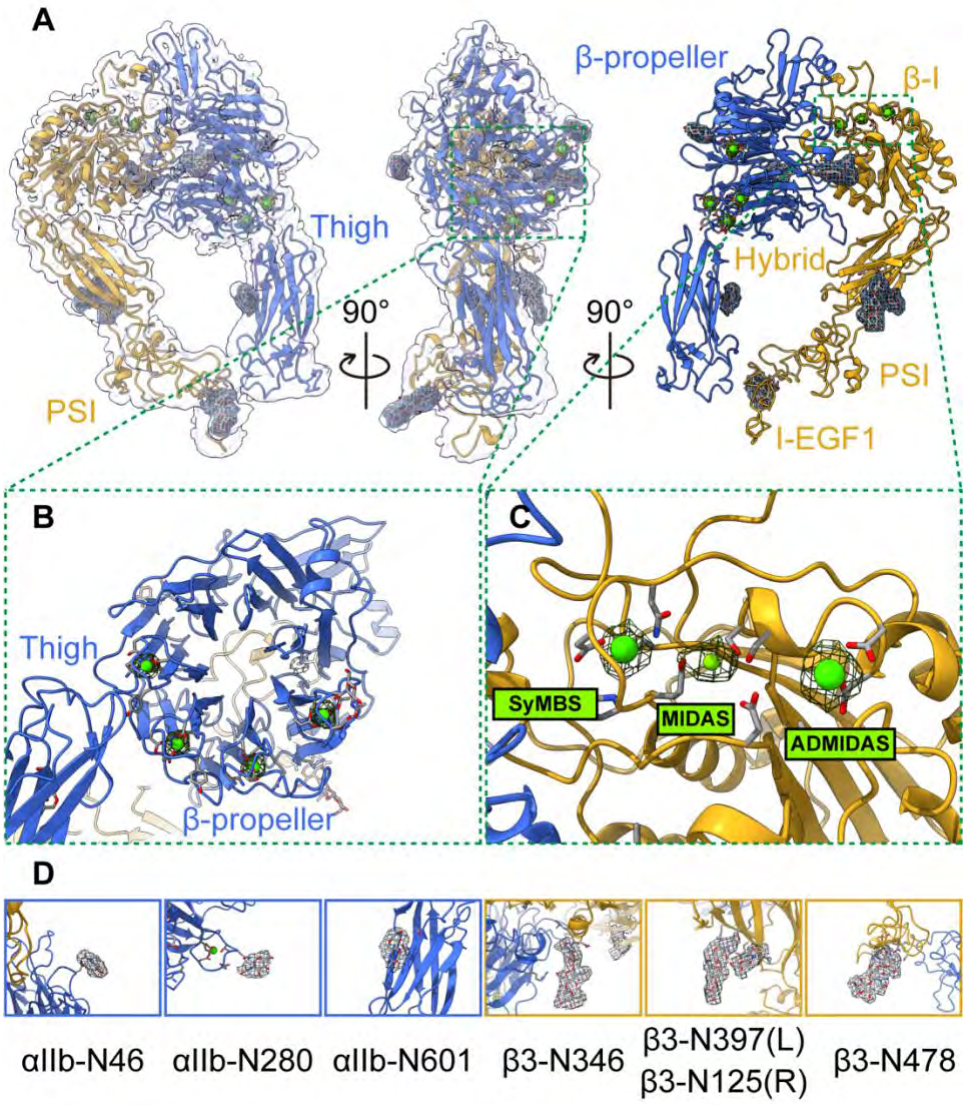

Figure 6

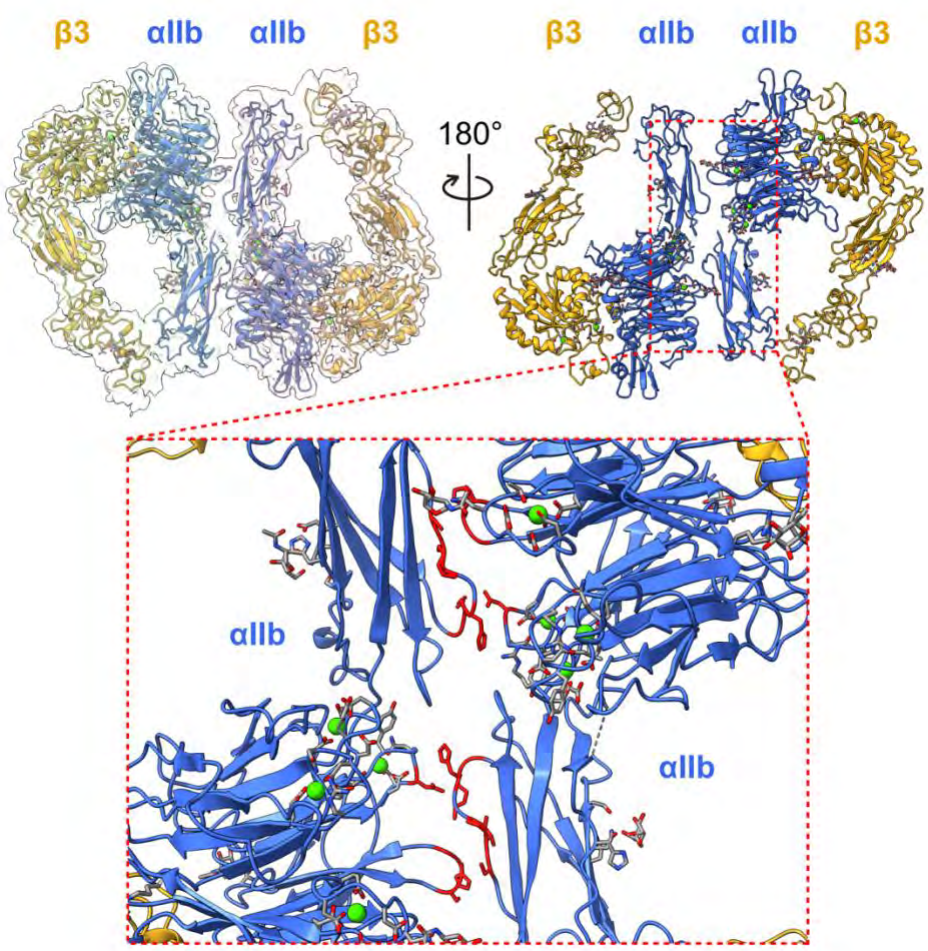

Figure 7

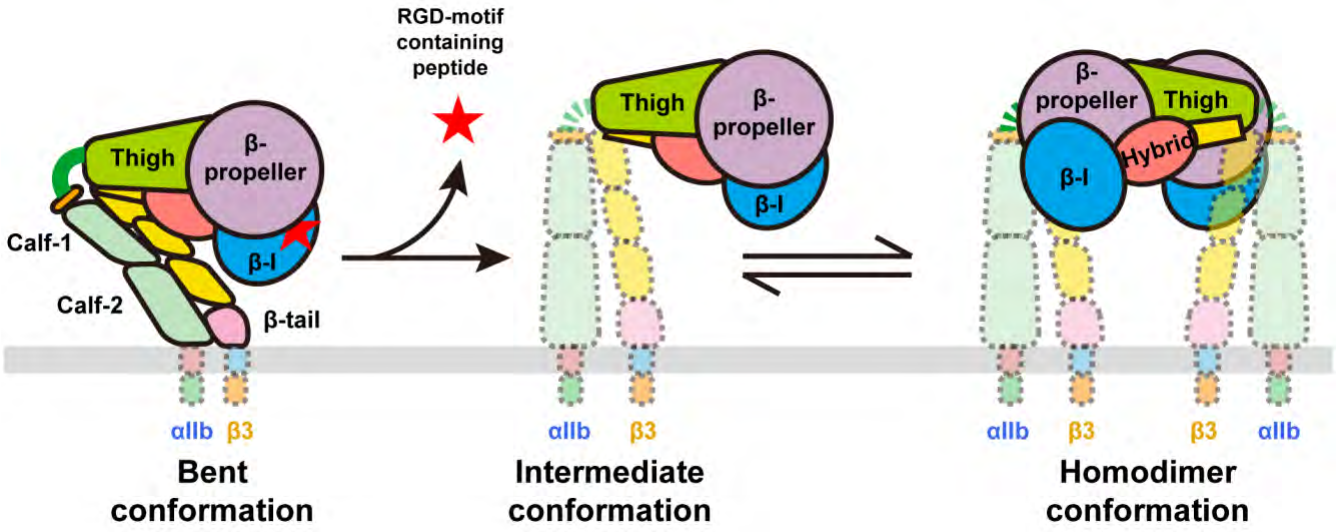

Supplemental Materials and methods

Preparation of human platelets

Blood was collected from healthy donors using butterfly needles into sodium citrate. Platelet-rich plasma (PRP) was obtained by centrifuging at 200g for 10 minutes followed by 10-minute incubation, both at room temperature. Platelet concentrations were determined using a Coulter Counter. Platelets were collected by an additional centrifugation at 2200g for 16 minutes.

Cryo-EM sample preparation

The pelleted human platelets were directly lysed by sonication in lysis buffer (phosphate buffer, 5 mM, pH 7.4) with protease inhibitor (Roche). The membrane fraction was collected by ultracentrifugation at 185,000g for 60 minutes at 4 °C. The membrane fraction was washed with high salt buffer (20 mM HEPES pH 7.5, 1M NaCl, 20 mM KCl, 10 mM $MgCl_2$) followed by low salt buffer (20 mM HEPES pH 7.5, 50 mM NaCl). The washed platelet membrane fraction was homogenized and solubilized in solubilization buffer (1% DDM, 0.1% CHS, 20 mM HEPES pH 7.5, 50 mM NaCl, 10% glycerol) with protease inhibitor cocktail overnight at 4 °C. The insoluble fraction was removed by ultracentrifugation at 185,000g for 60 minutes at 4 °C. Sample was then concentrated, passed through a 0.22 µm centrifugal filter, and enriched using size-exclusion chromatography (Superose 6 increase 10/300, GE Healthcare). Protein sizes corresponding to 200–550 kDa were collected and assembled into lipidic nanodiscs (MSP1E3D1; POPC:POPZ:POPG). The sample was then passed through a 0.22 µm centrifugal filter and enriched using size-exclusion chromatography (Superose 6 increase, GE Healthcare). Protein sizes corresponding to 200–350 kDa were used for cryo-EM analysis. A sample of 2.5 µL (5 mg/mL) was applied to Quantifoil R 1.2/1.3 Cu 300 holey grids. Samples were blotted for 16 s and plunged frozen into liquid ethane using a Vitrobot (Thermo Fisher). The resulting grids were stored in liquid nitrogen until data collection.

Data collection

A Titan Krios equipped with a K3 direct electron detector was used to collect data in super-resolution mode at 81,000 magnifications (physical pixel size of 1.070 Å/pix, 0.535 Å /pix super-resolution). Data were collected in correlated-double sampling mode using Serial EM.

Data processing

Data were processed in the cryoSPARC V4.6.0 suite using the BaR protocol as described previously.[1-5] The detailed data processing strategies are described in the Supplemental Data.

Protein Identification, model building and refinement

The near-atomic-resolution cryo-EM maps were used for protein identification using the online server DeepTracer™ and the program phenix.sequence_from_map in the PHENIX suite.[3,6,7] Initial models were built using the AlphaFold [8,9] via the UniProt database and aligned to the cryo-EM maps in Chimera. Models were refined using phenix.real_space_refine and Coot. Final structures were evaluated using MolProbity. 3D FSC was used to quantitatively evaluate each cryo-EM map at distinct viewing directions.

Quantification and statistical analysis

Standard GS-FSC (Gold Standard-Fourier Shell Correlation) curves at a threshold of 0.143 were computed using cryoSPARC v4.6.0 to obtain the final resolutions of protein models. The final atomic models were evaluated using MolProbity.

Proteomic analysis of platelet membrane fractions

The platelet membrane proteins in lipidic nanodiscs from the size-exclusion chromatography enrichment was digested by trypsin. The resulting peptides were desalted by a C18 Microspin column (Nest Group, Ipswich, MA) per the manufacturer's instructions and analyzed by LC-MS/MS using a ThermoScientific Fusion Lumos mass spectrometry system. Proteins were identified by comparing all experimental peptide MS/MS spectra against the UniProt human database using the Andromeda search engine integrated into the MaxQuant version 1.6.3.3. Carbamidomethylation of cysteine was set as a fixed modification, whereas variable modifications included oxidation of methionine to methionine sulfoxide and acetylation of N-terminal amino groups. For peptide/protein identification, strict trypsin specificity was applied, the minimum peptide length was set to 7, the maximum missed cleavage was set to 2, and the cutoff false discovery rate was set to 0.01. Match between runs (match time window: 0.7 min; alignment time window: 20 min) and label-free quantitation (LFQ) options were enabled. The LFQ minimum ratio count was set to 2. The remaining parameters were kept as default.

Supplemental Figure 1

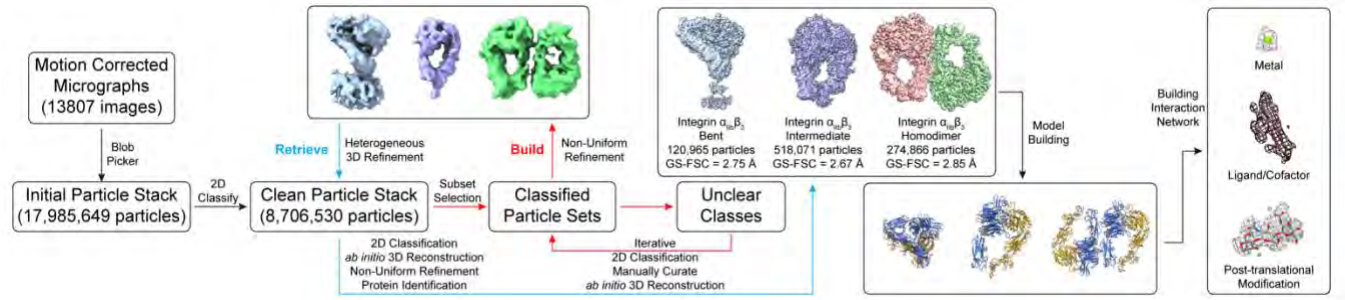

Supplemental Figure 1. The Build-and-Retrieve (BaR) data processing method workflow. An unbiased blob picker was applied on 13807 motion-corrected micrographs to generate 17,985,649 initial particles. The 2D classification was used to generate a subset of a clean particle stack that contains 8,706,530 particles. Classes of particles that contain clear 2D features were used to *Build* the low-resolution initial models, which were used to *Retrieve* more particles from the clean particle stack. The improved maps at ~3 Å resolution were used for protein identification. Final maps were used for model building and refinement.

Supplemental Figure 2

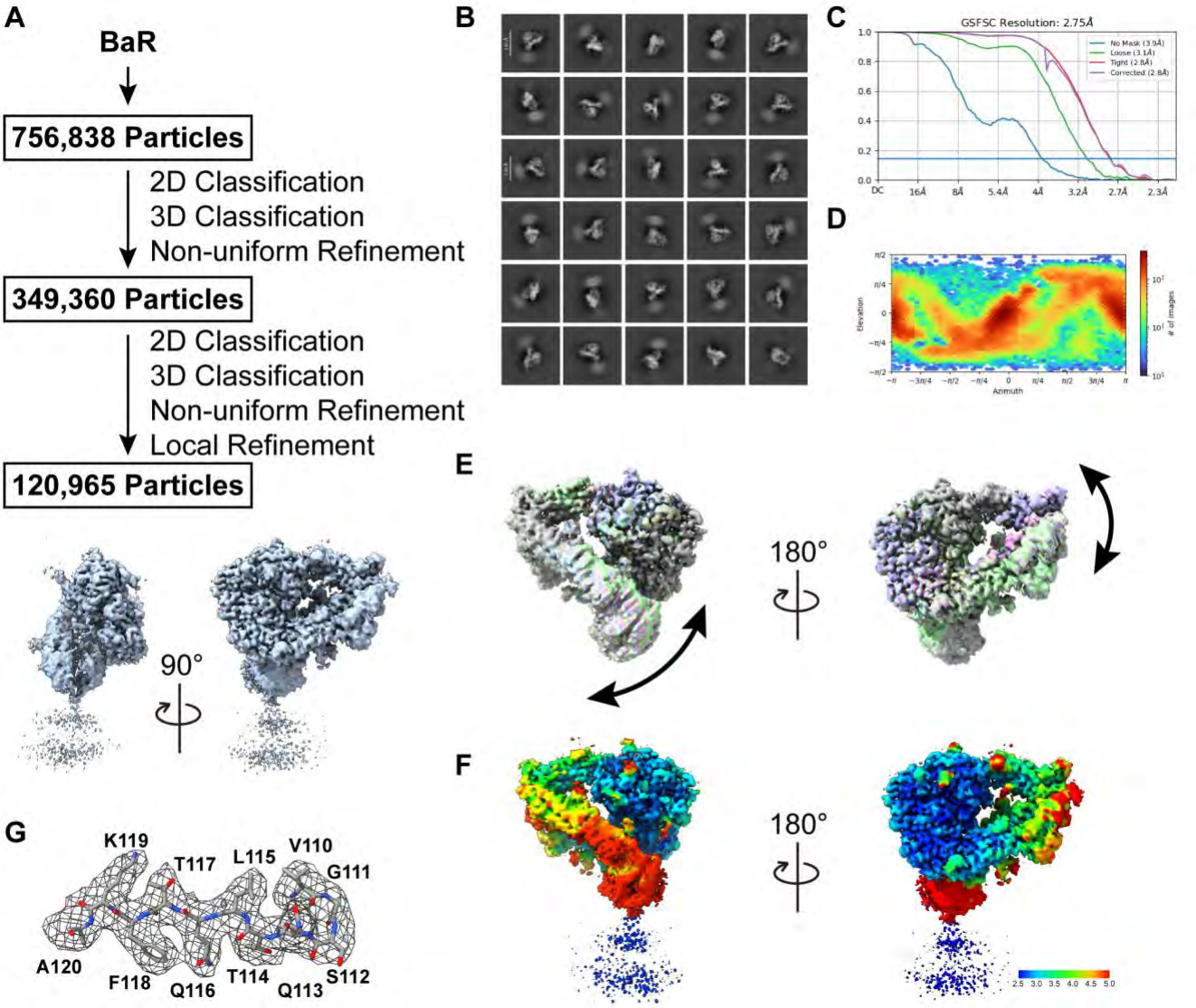

Supplemental Figure 2. Cryo-EM analysis of bent integrin αIIbβ3. A. Bent integrin αIIbβ3 particles processing flowchart. **B.** Representative 2D classes of bent integrin αIIbβ3. **C.** Fourier Shell Correlation (FSC) curves. **D.** Angular distribution calculated from cryoSPARC for particle projection. **E.** 3DFlex analysis shows the domain dynamic of integrin αIIbβ3 in the bent conformation. **F.** Cryo-EM density map of bent integrin αIIbβ3 colored by local resolution. **G.** Local density map of bent integrin αIIbβ3.

Supplemental Figure 3

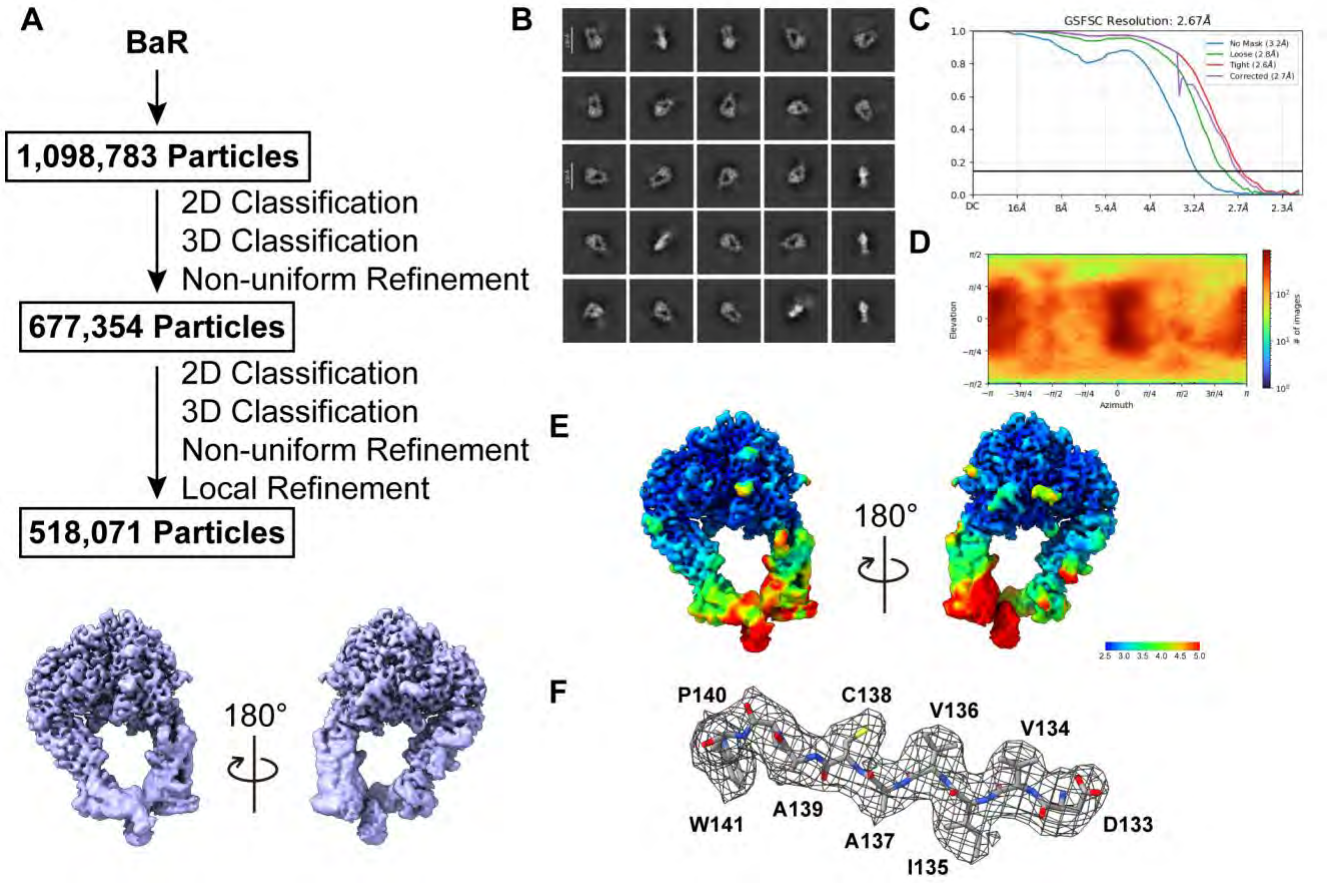

Supplemental Figure 3. Cryo-EM analysis of intermediate integrin αIIbβ3. A. Intermediate integrin αIIbβ3 particles processing flowchart. **B.** Representative 2D classes of intermediate integrin αIIbβ3. **C.** Fourier Shell Correlation (FSC) curves. **D.** Angular distribution calculated from cryoSPARC for particle projection. **E.** Cryo-EM density map of intermediate integrin αIIbβ3 colored by local resolution. **F.** Local density map of intermediate integrin αIIbβ3.

Supplemental Figure 4

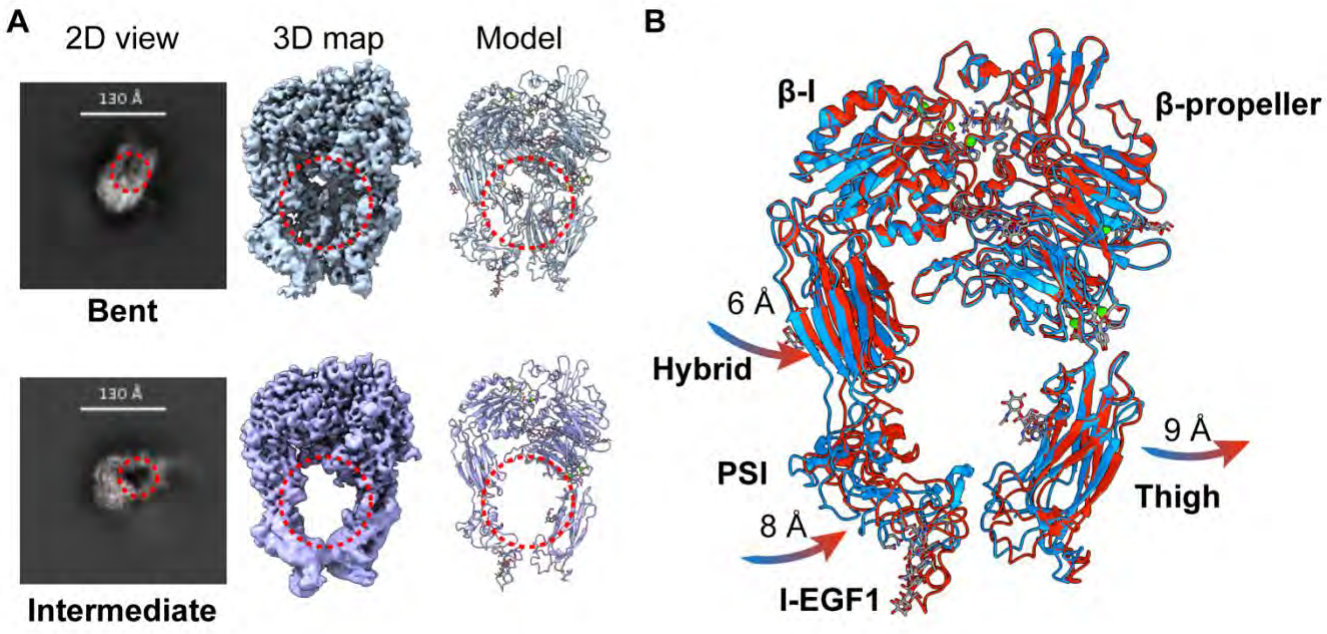

Supplemental Figure 4. Comparison of the integrin αIIbβ3 in bent and intermediate conformations. A. An additional density (red circle) can be observed in the 2D projection of the top view of the bent conformation but not in the intermediate state. This is the density of the lower leg region of the molecule, seeing through the headpiece in the 3D map and the final model. **B.** Overlay of the bent (blue) and intermediate (red) headpieces conformations demonstrates the domain movement between states.

Supplemental Figure 5

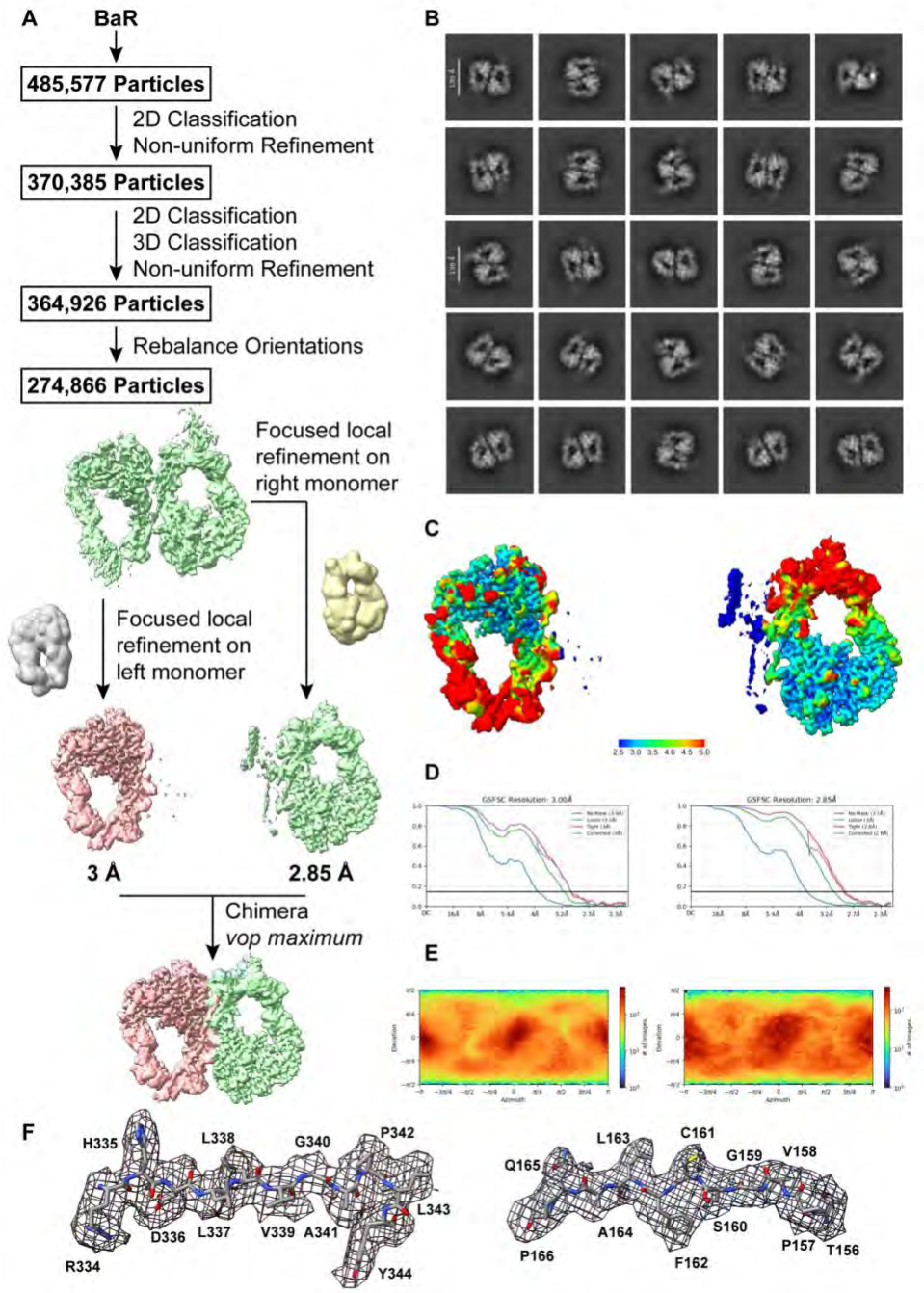

Supplemental Figure 5. Cryo-EM analysis of integrin αIIbβ3 homodimer. A. integrin αIIbβ3 homodimer particles processing flowchart. **B.** Representative 2D classes of dimer integrin αIIbβ3. **C.** Cryo-EM density map of dimer integrin αIIbβ3 colored by local resolution. **D.** Fourier Shell Correlation (FSC) curves. **E.** Angular distribution calculated from cryoSPARC for particle projection. **F.** Local density map of integrin αIIbβ3 homodimer.

References

1. Lyu M, Su CC, Miyagi M, Yu EW. Simultaneous solving high-resolution structures of various enzymes from human kidney microsomes. *Life Sci Alliance*. 2023;6(2).

2. Morgan CE, Zhang Z, Miyagi M, Golczak M, Yu EW. Toward structural-omics of the bovine retinal pigment epithelium. *Cell Rep*. 2022;41(13):111876.

3. Su CC, Lyu M, Morgan CE, Bolla JR, Robinson CV, Yu EW. A 'Build and Retrieve' methodology to simultaneously solve cryo-EM structures of membrane proteins. *Nat Methods*. 2021;18(1):69-75.

4. Su CC, Lyu M, Zhang Z, et al. High-resolution structural-omics of human liver enzymes. *Cell Rep*. 2023;42(6):112609.

5. Tringides ML, Zhang Z, Morgan CE, Su CC, Yu EW. A cryo-electron microscopic approach to elucidate protein structures from human brain microsomes. *Life Sci Alliance*. 2023;6(2).

6. Chang L, Wang F, Connolly K, et al. DeepTracer-ID: De novo protein identification from cryo-EM maps. *Biophys J*. 2022;121(15):2840-2848.

7. Pfab J, Phan NM, Si D. DeepTracer for fast de novo cryo-EM protein structure modeling and special studies on CoV-related complexes. *Proc Natl Acad Sci U S A*. 2021;118(2).

8. Abramson J, Adler J, Dunger J, et al. Accurate structure prediction of biomolecular interactions with AlphaFold 3. *Nature*. 2024.

9. Jumper J, Evans R, Pritzel A, et al. Highly accurate protein structure prediction with AlphaFold. *Nature*. 2021;596(7873):583-589.

Table 1: Cryo-EM data collection, processing, and refinement statistics

Data set	Bent conformation	Intermediate conformation	Homodimer conformation
Data collection and processing			
Magnification	81,000		
Votage (kV)	300		
Electron Microscope	Krios-GIF-K3		
Defocus range	- 0.8 ~ - 1.5		
Total Exposure time (s)	4s		
Pixel size (Å)	1.07		
Total dose (e-/A2)	37.3		
Number of frames	40		
Dose rate (e-/phys. Pixel/s)	11.71		
No. of initial micrographs	13,807		
No. of initial particles	17,985,649		
No. of final particles	120,965	518,071	274,866
Symmetry	C1	C1	C1
GSFSC Resolution (Å)	2.75	2.67	2.85
FSC threshold	0.143		
Refinement			
Initial model	Alphafold		
Model resolution cut-off (Å)	0.1	0.1	0.1
No. of Protein residues	1602	1106	2196
No. of ligands	Ca 7	Ca 6	Ca 12
	Mg 1	Mg 1	Mg 2
	NAG 18	NAG 10	NAG 18
	BMA 4	BMA 3	BMA 3
RMSD			
Bond lengths (Å)	0.005	0.007	0.004
Bond angles (°)	0.704	0.861	0.650
Validation			
MolProbity score	2.56	2.13	2.66
Clash score	25.16	10.81	15.26
Rotamer outliers (%)	2.49	1.73	4.59
Ramachandran plot (%)			
Favored (%)	94.59	94.19	92.49
Allowed (%)	5.22	5.63	7.19
Disallowed (%)	0.19	0.18	0.32

Table 2: Top 35 proteins in the Mass Spec Study

Protein IDs (Uniprot)	Protein names	Gene names	Mol. weight [kDa]	MS/MS count	iBAQ (High to Low)	Peptides	Sequence coverage [%]
P02647	Apolipoprotein A-I	APOA1	30.777	324	28.08583	42	83.1
P05106	Integrin beta-3	ITGB3	87.057	1076	28.03847	59	63.8
P08514	Integrin alpha-IIb	ITGA2B	113.38	1856	26.63339	64	52.6
P27105	Erythrocyte band 7 integral membrane protein	STOM	31.73	172	26.43232	18	72.9
P02776	Platelet factor 4	PF4	10.845	32	26.42886	6	36.6
Q93084	Sarcoplasmic/endoplasmic reticulum calcium ATPase 3	ATP2A3	109.25	349	26.30055	56	48.9
P16671	Platelet glycoprotein 4	CD36	53.053	111	26.13606	20	37.1
P13224	Platelet glycoprotein Ib beta chain	GP1BB	21.717	21	26.11728	6	23.8
P21926	CD9 antigen	CD9	25.416	28	26.07696	4	15.4
P14406	Cytochrome c oxidase subunit 7A2, mitochondrial	COX7A2	9.3959	11	25.94474	3	27.7
P09669	Cytochrome c oxidase subunit 6C	COX6C	8.7813	10	25.89647	5	38.7
P02675;CON__P02676	Fibrinogen beta chain	FGB	55.928	347	25.84125	48	76.8
P06576	ATP synthase subunit beta, mitochondrial	ATP5B	56.559	314	25.5996	29	73.7
P25705	ATP synthase subunit alpha, mitochondrial	ATP5A1	59.75	238	25.54687	49	66.9
P61224;A6NIZ1	Ras-related protein Rap-1b	RAP1B	20.825	60	25.5407	13	67.4
P14770	Platelet glycoprotein IX	GP9	19.046	41	25.51761	6	30.5
P02679	Fibrinogen gamma chain	FGG	51.511	215	25.49344	38	72
P05556	Integrin beta-1	ITGB1	88.414	223	25.41561	43	47.6
P62873;P16520	Guanine nucleotide-binding protein G(I)/G(S)/G(T) subunit beta-1	GNB1	37.377	80	25.26481	19	73.2
P56385	ATP synthase subunit e, mitochondrial	ATP5I	7.9331	27	25.21097	7	71

P48047	ATP synthase subunit O, mitochondrial	ATP5O	23.277	63	25.20202	15	75.1
P20674	Cytochrome c oxidase subunit 5A, mitochondrial	COX5A	16.762	26	25.16779	7	38
P07359	Platelet glycoprotein Ib alpha chain	GP1BA	71.539	76	25.16177	15	21.3
O75947	ATP synthase subunit d, mitochondrial	ATP5H	18.491	67	25.00774	14	84.5
P30273	High affinity immunoglobulin epsilon receptor subunit gamma	FCER1G	9.6674	8	24.9812	3	30.2
P04899;P11488;P19087;A8MTJ3;P09471	Guanine nucleotide-binding protein G(i) subunit alpha-2	GNAI2	40.45	148	24.9715	29	72.4
P16284	Platelet endothelial cell adhesion molecule	PECAM1	82.521	248	24.93656	40	53.5
Q9Y490;Q9Y4G6	Talin-1	TLN1	269.76	820	24.70055	156	73.4
P02489	Alpha-crystallin A chain	CRYAA	19.909	54	24.5251	7	36.4
P14625;Q58FF3	Endoplasmin	HSP90B1	92.468	172	24.4853	43	53.1
O75964	ATP synthase subunit g, mitochondrial	ATP5L	11.428	23	24.46251	6	52.4
P23229	Integrin alpha-6	ITGA6	126.6	233	24.35824	56	50
Q9Y277	Voltage-dependent anion-selective channel protein 3	VDAC3	30.658	53	24.32423	14	62.2
P40197	Platelet glycoprotein V	GP5	60.958	134	24.23783	24	50.5
P21333;Q14315;O75369	Filamin-A	FLNA	280.74	658	24.2292	155	61.5

Table 3: Peptide identified for ITGA2B and ITGB3

Integrin αIIb Peptide list

Sequence	Length	Missed cleavages	Mass	Proteins	Leading razor protein	Start position	End position	Gene names	Protein names	Unique (Groups)	Unique (Proteins)	Charges	PEP	Score	Experiment membrane_high MW	Experiment membrane_low MW	Intensity	Intensity membrane_high MW
AEAQVELRGNSFPASLVVAAEEGEREQNSLDSWGPK	36	2	3869.882	P08514	P08514	775	810	ITGA2B	Integrin alpha	yes	yes	4	1.22E-09	80.751	1	1	11513000	2605400
AEGGQCPSLLFDLR	14	0	1561.7559	P08514	P08514	91	104	ITGA2B	Integrin alpha	yes	yes	2;3	3.85E-92	238.92	2	1	353250000	271330000
AEGGQCPSLLFDLRDETR	18	1	2062.9742	P08514	P08514	91	108	ITGA2B	Integrin alpha	yes	yes	2	7.59E-28	186.51	1	1	717500000	396690000
AEGGQCPSLLFDLRDETRNVGSQTLQTFK	29	2	3266.599	P08514	P08514	91	119	ITGA2B	Integrin alpha	yes	yes	3;4	4.47E-07	95.209		2	291550000	0
AEYSPCRGNTLSR	13	1	1509.6994	P08514	P08514	172	184	ITGA2B	Integrin alpha	yes	yes	2	0.00039857	126.03	1	1	185820000	50223000
ALSNVEGFER	10	0	1120.5513	P08514	P08514	693	702	ITGA2B	Integrin alpha	yes	yes	2	0.046208	58.699	1		6349800	6349800
ARQGLGASVVSWSDVIVACAPWQHWNVLEK	30	1	3362.6982	P08514	P08514	120	149	ITGA2B	Integrin alpha	yes	yes	3;4	2.94E-17	122.38	1	2	24086000	3817600
ASVQLLVQDSLNPAVK	16	0	1680.941	P08514	P08514	487	502	ITGA2B	Integrin alpha	yes	yes	2;3	7.30E-41	223.22	61	56	465830000	243490000
DETRNVGSQTLQTFK	15	1	1722.8537	P08514	P08514	105	119	ITGA2B	Integrin alpha	yes	yes	2;3	1.11E-48	201.3	1	2	63688000	6681000
DGYNDIAVAAPYGGPSGR	18	0	1778.8224	P08514	P08514	400	417	ITGA2B	Integrin alpha	yes	yes	2;3	1.43E-59	211.7	2	2	140310000	81551000
DSHGRVAIVVGAPR	14	1	1432.7899	P08514	P08514	59	72	ITGA2B	Integrin alpha	yes	yes	3	0.030007	73.219		1	4628700	0
FGSAIAPLGDLDR	13	0	1330.6881	P08514	P08514	387	399	ITGA2B	Integrin alpha	yes	yes	2	1.08E-07	145.28	1	1	212560000	130670000
FGSAIAPLGDLDRDGYNDIAVAAPYGGPSGR	31	1	3091.4999	P08514	P08514	387	417	ITGA2B	Integrin alpha	yes	yes	3;4	3.30E-08	91.655	8	9	894460000	534110000
AIAPLGDLDRDGYNDIAVAAPYGGPSGRGQVLVFLGQSI	45	2	4575.3146	P08514	P08514	387	431	ITGA2B	Integrin alpha	yes	yes	4	1.11E-14	80.695		1	23969000	0
GAVDIDDNGYPDLIVGAYGANQVAVYR	27	0	2824.3668	P08514	P08514	454	480	ITGA2B	Integrin alpha	yes	yes	2;3	9.87E-101	234.36	9	22	664580000	208440000
GAVDIDDNGYPDLIVGAYGANQVAVYRAQPVVK	33	1	3446.747	P08514	P08514	454	486	ITGA2B	Integrin alpha	yes	yes	3	1.68E-28	138.23		1	2162700	0
GEAQVWTQLLR	11	0	1299.6935	P08514	P08514	978	988	ITGA2B	Integrin alpha	yes	yes	2	0.0012668	113.44	1	1	39765000	33060000
GEQMASYFGHSVAVTDVNGDGR	22	0	2296.0179	P08514	P08514	313	334	ITGA2B	Integrin alpha	yes	yes	3	0.0014796	81.226		1	4674200	0
GEQMASYFGHSVAVTDVNGDGRHDLLVGAPLYMESR	36	1	3877.8152	P08514	P08514	313	348	ITGA2B	Integrin alpha	yes	yes	4;5	7.69E-16	104.84	2	2	275080000	136960000
GNSFPASLVVAAEEGER	17	0	1731.8428	P08514	P08514	783	799	ITGA2B	Integrin alpha	yes	yes	2;3	1.04E-158	307.43	2	1	47018000	34059000
GNSFPASLVVAAEEGEREQNSLDSWGPK	28	1	2973.4104	P08514	P08514	783	810	ITGA2B	Integrin alpha	yes	yes	2;3;4	1.30E-30	154.31	3	4	1049900000	699880000
GPHALGAPSLLLTGTQLYGR	20	0	2021.1058	P08514	P08514	367	386	ITGA2B	Integrin alpha	yes	yes	2;3	4.12E-60	225.21	2	3	1084600000	592590000
GQVLVFLGQSEGLR	14	0	1501.8253	P08514	P08514	418	431	ITGA2B	Integrin alpha	yes	yes	2;3	2.60E-39	203.51	67	71	155300000	66567000
HDLLVGAPLYMESR	14	0	1599.8079	P08514	P08514	335	348	ITGA2B	Integrin alpha	yes	yes	2;3	2.91E-13	158.06	2	2	131030000	85886000
HSPICHTTMAFLR	13	0	1569.7544	P08514	P08514	572	584	ITGA2B	Integrin alpha	yes	yes	2;3	0.0065149	92.792	2	1	165960000	114990000
HSPICHTTMAFLRDEADFRDK	21	2	2546.1795	P08514	P08514	572	592	ITGA2B	Integrin alpha	yes	yes	3;4;5	0.021731	61.096	4	1	3962800000	2990200000
IVLLDVPVR	9	0	1022.6488	P08514	P08514	766	774	ITGA2B	Integrin alpha	yes	yes	2	0.00021556	127.56		1	204610000	0
IVLLDVPVRAEAQVELR	17	1	1919.1204	P08514	P08514	766	782	ITGA2B	Integrin alpha	yes	yes	2;3	0.0036604	118.08	11	13	449660000	235890000
IYVENDFSWDK	11	0	1414.6405	P08514	P08514	185	195	ITGA2B	Integrin alpha	yes	yes	2	1.29E-16	172.21	50	38	1355000000	1327100000
IYVENDFSWDKR	12	1	1570.7416	P08514	P08514	185	196	ITGA2B	Integrin alpha	yes	yes	2;3	9.42E-88	202.31	2	2	2077900000	1084800000
KLAEVGRVYLFLQPR	15	2	1788.041	P08514	P08514	352	366	ITGA2B	Integrin alpha	yes	yes	3	0.0086289	79.886		1	4028200	0
LAEVGRVYLFLQPR	14	1	1659.9461	P08514	P08514	353	366	ITGA2B	Integrin alpha	yes	yes	2;3	3.67E-05	127.51		2	130210000	0
LQDPVLVSCDSAPCTVVQCDLQEMAR	26	0	2990.3606	P08514	P08514	903	928	ITGA2B	Integrin alpha	yes	yes	2;3	6.18E-54	182.47	7	5	936850000	601810000
LQDPVLVSCDSAPCTVVQCDLQEMARGQR	29	1	3331.5418	P08514	P08514	903	931	ITGA2B	Integrin alpha	yes	yes	3	1.36E-05	84.365		1	4495900	0
LRGEQMASYFGHSVAVTDVNGDGR	24	1	2565.203	P08514	P08514	311	334	ITGA2B	Integrin alpha	yes	yes	3	5.67E-06	96.723	1	1	38141000	24621000
RGEQMASYFGHSVAVTDVNGDGRHDLLVGAPLYMESI	38	2	4147.0004	P08514	P08514	311	348	ITGA2B	Integrin alpha	yes	yes	4;5;6	2.06E-21	112.12	5	5	3598700000	2788100000
LSLNAELQLDR	11	0	1270.6881	P08514	P08514	533	543	ITGA2B	Integrin alpha	yes	yes	2	1.02E-104	251.43	49	62	1171100000	611870000
LSLNAELQLDRQKPR	15	2	1779.9955	P08514	P08514	533	547	ITGA2B	Integrin alpha	yes	yes	3;4	0.037557	61.212		2	66086000	0
NRPPLEEDDEEGE	13	1	1527.6325	P08514	P08514	1027	1039	ITGA2B	Integrin alpha	yes	yes	2	7.85E-34	172.56	1	1	6921100	4769100
NVGSQTLQTFK	11	0	1221.6354	P08514	P08514	109	119	ITGA2B	Integrin alpha	yes	yes	2	0.0013713	102.95	1	1	8551500	4970300
NVGSQTLQTFKAR	13	1	1448.7736	P08514	P08514	109	121	ITGA2B	Integrin alpha	yes	yes	2	0.015723	68.132		1	3844800	0
PSQVLDSPFPTGSAFGFSLR	20	0	2109.0531	P08514	P08514	434	453	ITGA2B	Integrin alpha	yes	yes	2	5.04E-105	239.19	1	1	4704700	2548400
QGLGASVVSWSDVIVACAPWQHWNVLEK	28	0	3135.56	P08514	P08514	122	149	ITGA2B	Integrin alpha	yes	yes	3;4	3.68E-23	134.42	1	2	56655000	10340000
QGLGASVVSWSDVIVACAPWQHWNVLEKTEEAEK	34	1	3822.8676	P08514	P08514	122	155	ITGA2B	Integrin alpha	yes	yes	4	9.64E-09	88.721		1	2039600	0
QIFLPEPEQPSR	12	0	1439.7409	P08514	P08514	891	902	ITGA2B	Integrin alpha	yes	yes	2	0.016211	69.346	1	1	10072000	7589600
QIFLPEPEQPSRLQDPVLVSCDSAPCTVVQCDLQEMAR	38	1	4412.0909	P08514	P08514	891	928	ITGA2B	Integrin alpha	yes	yes	3;4	3.10E-08	63.44	2	1	35657000	19994000
RAEYSPCRGNTLSR	14	2	1665.8005	P08514	P08514	171	184	ITGA2B	Integrin alpha	yes	yes	3	0.020198	91.62	1		307540000	307540000
RVLLLGSQQAGTTLNLDLGGK	21	1	2153.2168	P08514	P08514	551	571	ITGA2B	Integrin alpha	yes	yes	2;3	4.37E-37	188.16	6	6	943420000	464880000
SCVLPQTK	8	0	931.4797	P08514	P08514	503	510	ITGA2B	Integrin alpha	yes	yes	2	5.27E-12	158.07	1		1252900000	1252900000
SCVLPQTKTPVSCFNIQMCVGATGHNIPQK	30	1	3371.6247	P08514	P08514	503	532	ITGA2B	Integrin alpha	yes	yes	3;4	3.79E-10	106.44	1	3	338250000	30207000
SRPSQVLDSPFPTGSAFGFSLR	22	1	2352.1862	P08514	P08514	432	453	ITGA2B	Integrin alpha	yes	yes	2;3;4	6.08E-95	274.81	11	10	1089000000	444670000
TEEAEKTPVGSCFLAQPESGR	21	1	2292.0692	P08514	P08514	150	170	ITGA2B	Integrin alpha	yes	yes	2;3	0	347.52	4	2	3271300000	2294000000
TEEAEKTPVGSCFLAQPESGRR	22	2	2448.1703	P08514	P08514	150	171	ITGA2B	Integrin alpha	yes	yes	2;3;4	1.18E-06	153.68	3	4	5533000000	3613300000
TLGPSQEETGGVFLCPWR	18	0	2032.9677	P08514	P08514	73	90	ITGA2B	Integrin alpha	yes	yes	2;3	1.36E-122	249.28	16	6	1276800000	850580000
TLGPSQEETGGVFLCPWRAEGGQCPSLLFDLR	32	1	3576.713	P08514	P08514	73	104	ITGA2B	Integrin alpha	yes	yes	3;4	1.59E-09	96.466	1	2	31653000	3501400
TLGPSQEETGGVFLCPWRAEGGQCPSLLFDLRDETR	36	2	4077.9313	P08514	P08514	73	108	ITGA2B	Integrin alpha	yes	yes	3;4;5	0.00017415	51.234	1	3	1070400000	4974700
TPVGSCFLAQPESGR	15	0	1604.7617	P08514	P08514	156	170	ITGA2B	Integrin alpha	yes	yes	2	2.25E-76	227.06	1	1	77679000	52872000
TPVGSCFLAQPESGRR	16	1	1760.8628	P08514	P08514	156	171	ITGA2B	Integrin alpha	yes	yes	2;3	3.34E-08	127.87	2		89255000	89255000
TPVSCFNIQMCVGATGHNIPQK	22	0	2458.1556	P08514	P08514	511	532	ITGA2B	Integrin alpha	yes	yes	2;3	5.50E-81	222.13	52	59	2869400000	1465200000
VAIVVGAPR	9	0	880.54944	P08514	P08514	64	72	ITGA2B	Integrin alpha	yes	yes	1;2	0.010423	101.21	1	2	98654000	0
VLLLGSQQAGTTLNLDLGGK	20	0	1997.1157	P08514	P08514	552	571	ITGA2B	Integrin alpha	yes	yes	2;3	0	373.06	31	40	1613800000	751540000
VVLCELGNPMK	11	0	1258.6414	P08514	P08514	715	725	ITGA2B	Integrin alpha	yes	yes	2	1.53E-07	152.97	1	2	394810000	254220000
VVLCELGNPMKK	12	1	1386.7363	P08514	P08514	715	726	ITGA2B	Integrin alpha	yes	yes	2;3	1.70E-16	172.98	3	5	2453500000	1475200000
VYLFLQPR	8	0	1034.5913	P08514	P08514	359	366	ITGA2B	Integrin alpha	yes	yes	2	1.88E-06	125.86	35	33	53494000	30845000

Integrin β3 Peptide list

Sequence	Length	Missed cleavages	Mass	Proteins	Leading razor protein	Start position	End position	Gene names	Protein names	Unique (Groups)	Unique (Proteins)	Charges	PEP	Score	Experiment membrane_high MW	Experiment membrane_low MW	Intensity	Intensity membrane_high MW
AKWDTANNPLYK	12	1	1419.7147	P05106	P05106	763	774	ITGB3	tegrin beta	yes	yes	2;3	0.0033346	120.63		2	22307000	0
CDLKENLLK	9	1	1131.5958	P05106	P05106	64	72	ITGB3	tegrin beta	yes	yes	2;3	4.18E-16	181.41	3	3	570960000	406310000
CDLKENLLKDNCAPESIEFPVSEAR	25	2	2933.3899	P05106	P05106	64	88	ITGB3	tegrin beta	yes	yes	2;3;4	8.07E-44	220.97	5	2	7085400000	5439700000
CECGSCVCIQPGSYGDTCEK	20	0	2365.8742	P05106	P05106	607	626	ITGB3	tegrin beta	yes	yes	2;3	1.67E-30	233.47	2	2	177910000	122530000
CECGSCVCIQPGSYGDTCEKCPTCPDACTFK	31	1	3703.3944	P05106	P05106	607	637	ITGB3	tegrin beta	yes	yes	3;4	9.14E-130	234.1	2	4	2508600000	1127000000
CECGSCVCIQPGSYGDTCEKCPTCPDACTFKK	32	2	3831.4894	P05106	P05106	607	638	ITGB3	tegrin beta	yes	yes	3;4	1.85E-16	117.15	2	2	510980000	216080000
CGPGWLGSQCECSEEDYRPSQQDECSPR	28	1	3373.3129	P05106	P05106	488	515	ITGB3	tegrin beta	yes	yes	3;4	1.10E-41	161.64	3	3	3694800000	1964400000
GPGWLGSQCECSEEDYRPSQQDECSPREGQPVCSQ	37	2	4414.779	P05106	P05106	488	524	ITGB3	tegrin beta	yes	yes	3;4	0.00090283	46.872	1	2	215940000	43577000
CNNGNGTFECGVCR	14	0	1643.6239	P05106	P05106	474	487	ITGB3	tegrin beta	yes	yes	2	7.04E-117	265	1	1	2142500	0
CPTCPDACTFK	11	0	1355.5308	P05106	P05106	627	637	ITGB3	tegrin beta	yes	yes	2	9.08E-71	230.06	1	2	639820000	458240000
CPTCPDACTFKK	12	1	1483.6258	P05106	P05106	627	638	ITGB3	tegrin beta	yes	yes	2;3	1.00E-16	194.48	2	2	108110000	78356000
DAPEGGFDAIMQATVCDEK	19	0	2052.8769	P05106	P05106	243	261	ITGB3	tegrin beta	yes	yes	2	4.77E-87	254.72	1	1	77661000	36621000
DDLWSIQNLGTK	12	0	1388.6936	P05106	P05106	152	163	ITGB3	tegrin beta	yes	yes	2;3	3.58E-148	270.61	2	2	1199400000	3995500
DEIESVKELK	10	1	1188.6238	P05106	P05106	663	672	ITGB3	tegrin beta	yes	yes	2;3	1.42E-32	185.81	2	2	130840000	115720000
DEIESVKELKDTGK	14	2	1589.8148	P05106	P05106	663	676	ITGB3	tegrin beta	yes	yes	3	0.055986	59.898		1	3120700	0
DNCAPESIEFPVSEAR	16	0	1819.8047	P05106	P05106	73	88	ITGB3	tegrin beta	yes	yes	2;3	1.93E-80	206.45	2	2	832040000	579680000
DSLIVQVTFDCDCACQAQAEPNSHR	25	0	2920.2538	P05106	P05106	449	473	ITGB3	tegrin beta	yes	yes	3	3.51E-28	148.69		1	2062900	0
EATSTFTNITYR	12	0	1402.6729	P05106	P05106	775	786	ITGB3	tegrin beta	yes	yes	2	1.00E-07	152.69	1	1	953110000	744070000
EATSTFTNITYRGT	14	1	1560.742	P05106	P05106	775	788	ITGB3	tegrin beta	yes	yes	2	8.99E-152	272.1	1	1	1042100000	601730000
EGQPVCSQRGECLCGQCVCHSSDFGK	26	1	3041.2307	P05106	P05106	516	541	ITGB3	tegrin beta	yes	yes	3;4	1.51E-54	186.68	2	2	3972400000	1285600000
ENLLKDNCAPESIEFPVSEAR	21	1	2417.1533	P05106	P05106	68	88	ITGB3	tegrin beta	yes	yes	2;3	1.10E-280	320	2	2	389440000	262740000
FDRGALHDENTCNR	14	1	1703.7434	P05106	P05106	646	659	ITGB3	tegrin beta	yes	yes	2;3;4	2.69E-60	239.48	4	3	2905500000	2047000000
FDRGALHDENTCNRYCR	17	2	2182.9385	P05106	P05106	646	662	ITGB3	tegrin beta	yes	yes	3;5	4.16E-17	158.93	2	2	63471000	35988000
GALHDENTCNRYCR	14	1	1764.742	P05106	P05106	649	662	ITGB3	tegrin beta	yes	yes	4	0.007986	63.473	1	1	44675000	34382000
GALHDENTCNRYCRDEIESVK	21	2	2565.1336	P05106	P05106	649	669	ITGB3	tegrin beta	yes	yes	3	7.60E-09	119.68	1	1	55443000	43649000
GECLCGQCVCHSSDFGK	17	0	1999.7645	P05106	P05106	525	541	ITGB3	tegrin beta	yes	yes	2;3	1.04E-158	276.32	2	2	3293700000	2008800000
GSGDSSQVTQVSPQR	15	0	1531.7227	P05106	P05106	99	113	ITGB3	tegrin beta	yes	yes	2	4.00E-131	259.75	2	2	200880000	8648700
GVSSCQQCLAVSPMCAWCSDEALPLGSPR	29	0	3222.4025	P05106	P05106	35	63	ITGB3	tegrin beta	yes	yes	3;4	2.65E-15	124.17	6	7	2917600000	1522600000
HVLTLTDQVTR	11	0	1281.7041	P05106	P05106	218	228	ITGB3	tegrin beta	yes	yes	2;3	1.73E-07	202.96	3	2	765730000	469330000
HVLTLTDQVTRFNEEVK	17	1	2028.064	P05106	P05106	218	234	ITGB3	tegrin beta	yes	yes	2;3;4	3.03E-207	299.04	3	4	1034700000	715750000
HVLTLTDQVTRFNEEVKK	18	2	2156.159	P05106	P05106	218	235	ITGB3	tegrin beta	yes	yes	3;4	2.89E-28	169.98	2	1	839230000	586100000
IGDTVSFSIEAK	12	0	1265.6503	P05106	P05106	417	428	ITGB3	tegrin beta	yes	yes	2	3.16E-45	208.33	78	73	395390000	190470000
IGFGAFVDKPVSPYMYISPPEALENPCYDMK	31	1	3534.655	P05106	P05106	177	207	ITGB3	tegrin beta	yes	yes	3;4	3.05E-36	144.44	9	10	2563000000	664950000
IGWRNDASHLLVFTTDAK	18	1	2043.0538	P05106	P05106	262	279	ITGB3	tegrin beta	yes	yes	2;3;4	2.55E-103	225.31	3	2	4830500000	2599500000
ITGKYCECDDFSCVR	15	1	1908.7805	P05106	P05106	542	556	ITGB3	tegrin beta	yes	yes	2;3	1.34E-228	311.54	2	2	3891100000	1149100000
KFDRGALHDENTCNR	15	2	1831.8384	P05106	P05106	645	659	ITGB3	tegrin beta	yes	yes	3;4	4.13E-06	127.05	2	2	400020000	152560000
LAGIVQPNDGQCHVGSDNHYSASTTMDYPSLGLMTEK	37	0	3992.7979	P05106	P05106	288	324	ITGB3	tegrin beta	yes	yes	3;4;5	1.17E-11	90.674	7	6	2085400000	1796300000
GIVQPNDGQCHVGSDNHYSASTTMDYPSLGLMTEKLS	41	1	4449.0675	P05106	P05106	288	328	ITGB3	tegrin beta	yes	yes	4	0.036144	26.399		1	3782700	0
NDASHLLVFTTDAK	14	0	1530.7678	P05106	P05106	266	279	ITGB3	tegrin beta	yes	yes	2;3	5.02E-76	231.74	2	3	2347000000	1596000000
NEDDCVVRFQYYEDSSGK	18	1	2209.9222	P05106	P05106	685	702	ITGB3	tegrin beta	yes	yes	2;3	2.80E-08	170.48	1	2	41249000	6848000
NRDAPEGGFDAIMQATVCDEK	21	1	2323.0209	P05106	P05106	241	261	ITGB3	tegrin beta	yes	yes	2;3	2.57E-79	258.12	53	61	2336200000	2138800000
NRDAPEGGFDAIMQATVCDEKIGWR	25	2	2835.3068	P05106	P05106	241	265	ITGB3	tegrin beta	yes	yes	3;4	1.03E-45	176.9	2	3	354760000	34771000
PLSDKGSGDSSQVTQVSPQR	20	1	2072.0134	P05106	P05106	94	113	ITGB3	tegrin beta	yes	yes	3	0.0014529	70.334	1		2379000	2379000
QVEDYPVDIYYLMDLSYSMK	20	0	2471.1277	P05106	P05106	132	151	ITGB3	tegrin beta	yes	yes	3	9.89E-19	144.74		1	2413700	0
QVEDYPVDIYYLMDLSYSMKDDLWSIQNLGTK	32	1	3841.8107	P05106	P05106	132	163	ITGB3	tegrin beta	yes	yes	3	8.11E-06	71.295	1		1505500	1505500
SFTIKPVGFK	10	1	1122.6437	P05106	P05106	439	448	ITGB3	tegrin beta	yes	yes	2;3	2.33E-06	147.19	2	2	2094400000	1501500000
SFTIKPVGFKDSLIVQVTFDCDCACQAQAEPNSHR	35	2	4024.887	P05106	P05106	439	473	ITGB3	tegrin beta	yes	yes	4;5	6.80E-30	141.38	2	3	128580000	55625000
TDTCMSSNGLLCSGR	15	0	1657.6858	P05106	P05106	590	604	ITGB3	tegrin beta	yes	yes	2	6.34E-258	323.44	9	10	1700500000	844090000
TTCLPMFGYK	10	0	1216.5621	P05106	P05106	208	217	ITGB3	tegrin beta	yes	yes	2	0.0020581	124.08	3	6	4414600000	2039400000
TTCLPMFGYKHVLTLTDQVTR	21	1	2480.2556	P05106	P05106	208	228	ITGB3	tegrin beta	yes	yes	3;4	0.0010891	122.13		2	27214000	0
TTCLPMFGYKHVLTLTDQVTRFNEEVK	27	2	3226.6155	P05106	P05106	208	234	ITGB3	tegrin beta	yes	yes	4	0.029545	37.209		1	13715000	0
VLEDRPLSDK	10	1	1170.6245	P05106	P05106	89	98	ITGB3	tegrin beta	yes	yes	2;3	9.55E-23	178.55	1	2	568280000	289200000
VLEDRPLSDKGSGDSSQVTQVSPQR	25	2	2684.3365	P05106	P05106	89	113	ITGB3	tegrin beta	yes	yes	2;3;4	3.81E-76	210.31	5	4	3236300000	2921300000
WDTANNPLYK	10	0	1220.5826	P05106	P05106	765	774	ITGB3	tegrin beta	yes	yes	2	0.010158	78.264	1		4867300	4867300
WDTANNPLYKEATSTFTNITYR	22	1	2605.2449	P05106	P05106	765	786	ITGB3	tegrin beta	yes	yes	2;3	1.32E-35	202.18	2	2	733040000	364160000
WDTANNPLYKEATSTFTNITYRGT	24	2	2763.314	P05106	P05106	765	788	ITGB3	tegrin beta	yes	yes	2;3	7.68E-37	156.29	2	2	273540000	254730000
YCECDDFSCVR	11	0	1509.5323	P05106	P05106	546	556	ITGB3	tegrin beta	yes	yes	2	4.76E-124	259.58	1	1	4654000000	2838100000
YCRDEIESVK	10	1	1297.5973	P05106	P05106	660	669	ITGB3	tegrin beta	yes	yes	2;3	8.14E-05	172.56	2	2	692440000	584280000
YCRDEIESVKELK	13	2	1667.8189	P05106	P05106	660	672	ITGB3	tegrin beta	yes	yes	2;3;4	4.08E-58	215.02	3	3	1495800000	1191100000

Intensity membrane_low MW	Reverse	Potential contaminant	id	Protein group IDs	Mod. peptide IDs	Evidence IDs	MS/MS IDs	Best MS/MS	Oxidation (M) site IDs	Taxonomy IDs	Mass deficit	MS/MS Count	LFQ intensity membrane_high MW	LFQ intensity membrane_low MW
8907600			149	263	150	290;291	0;421;422;4	423			0.061878	4	2605400	16403000
81920000			160	263	161	306;307;308	445;446;447	444			-0.00253	9	271330000	150850000
320810000			161	263	162	309;310	451;452	451			-0.01477	2	396690000	590770000
291550000			162	263	163	311;312	453;454;455	455			0.056353	2	0	536880000
135590000			189	263	192	366;367	528;529	528			-0.03504	2	50223000	249690000
0			459	263	470	947	1417;1418	1417			-0.00417	2	6349800	0
20268000			619	263	637	251;1252;12	;1843;1844;	1844			0.111408	4	3817600	37324000
222330000			688	263	707	452;1453;14	49;2150;21	2063			0.127802	228	243490000	409430000
57006000			1137	263	1168	414;2415;24	;3665;3666;	3666			0.021164	4	6681000	104980000
58757000			1201	263	1234	;2539;2540;	;3834;3835;	3833			-0.03588	4	81551000	108200000
4628700			1381	263	1415	2871	4294	4294			0.090811	1	0	8523600
81890000			1920	263	1962	3872;3873	720;5721;57	5720			0.035998	7	130670000	150800000
360350000			1921	263	1963	881;3882;388	;5745;5746;	5725			0.037837	41	534110000	663580000
23969000			1922	263	1964	3891	5767;5768	5768			0.169994	2	0	44138000
456140000			2200	263	2251	466;4467;44	;6658;6659;	6628			0.027579	65	208440000	839980000
2162700			2201	263	2252	4483	6692;6693	6693			0.12153	2	0	3982600
6705200			2242	263	2293	4551;4552	;6788;6789;	6789			0.055676	4	33060000	12347000
4674200			2258	263	2309	4578	6819	6819			-0.07831	1	0	8607400
138120000			2259	263	2310	;4580;4581;	;6823;6824;	6825			-0.00859	8	136960000	254350000
12959000			2481	263	2535	999;5000;50	;7400;7401;	7405			0.00613	12	34059000	23863000
349970000			2482	263	2536	004;5005;50	418;7419;74	7417			0.002674	25	699880000	644460000
492030000			2495	263	2549	039;5040;50	494;7495;74	7497			0.1361	11	592590000	906070000
88732000			2526	263	2580	;5161;5162;	677;7678;76	7805			0.094437	238	66567000	163400000
45140000			2750	263	2809	;5654;5655;	441;8442;84	8444			0.032001	5	85886000	83125000
50969000			2889	263	2952	935;5936;59	871;8872;88	8872			-0.00765	3	114990000	93859000
972530000			2890	263	2953;2954	939;5940;59	;8876;8877;	8875	69		-0.03178	6	2990200000	1790900000
204610000			3497	263	3572	7310	70;10971;10	10970			0.138398	3	0	376790000
213780000			3498	263	3573	;7322;7323;	89;10990;10	11004			0.197601	21	235890000	393670000
27894000			3556	263	3632	;7481;7482;	32;11233;11	11150			-0.05024	169	1327100000	51367000
993110000			3557	263	3633	;7527;7528;	11325;11326	11327			-0.02093	16	1084800000	1828800000
4028200			3743	263	3823	7930	11932	11932			0.178525	1	0	7417800
130210000			3918	263	4006	8339;8340	12520;12521	12524			0.142486	8	0	239770000
335040000			4541	263	4645;4646	;9566;9567;	14350;14351	14356	70		-0.05497	20	601810000	616970000
4495900			4542	263	4647	9573	14361;14362	14361			-0.03076	2	0	8279200
13520000			4613	263	4718	9708;9709	56;14557;14	14556			-0.01696	5	24621000	24896000
810560000			4614	263	4719;4720	;9714;9715;	14566;14567	14573	71;72		0.052761	14	2788100000	1492600000
559230000			4672	263	4778	889;9890;98	821;14822;1	14738			0.063598	186	611870000	1029800000
66086000			4673	263	4779	9946;9947	14923;14924	14923			0.136732	1	0	121700000
2152000			5449	263	5616	11650;11651	17446;17447	17447			-0.1102	2	4769100	3962900
3581200			5516	263	5684	11764;11765	17618;17619	17619			0.033399	2	4970300	6594700
3844800			5517	263	5685	11766	17620	17620			0.06714	1	0	7080100
2156400			5588	263	5756	11907;11908	28;17829;17	17829			0.04294	3	2548400	3970900
46315000			5689	263	5859	99;12100;12	18085;18086	18082			0.077667	8	10340000	85289000
2039600			5690	263	5860	12102	90;18091;18	18090			0.06904	3	0	3755900
2482500			5715	263	5886	12157;12158	18169;18170	18170			0.038598	2	7589600	4571500
15663000			5716	263	5887	59;12160;12	18172;18173	18173			0.02135	4	19994000	28843000
0			5910	263	6081	12499	18643	18643			-0.00573	1	307540000	0
478540000			6155	263	6330	13007;13008	63;19364;19	19353			0.186336	23	464880000	881230000
0			6248	263	6426	13187	10;19611;19	19611			0.011221	3	1252900000	0
308050000			6249	263	6427;6428	13189;13190	19616;19617	19617	73		0.033745	8	30207000	567260000
644340000			6646	263	6832	83;13984;13	398;20799;20	20801			0.064239	32	444670000	1186500000
977250000			6903	263	7097	14512;14513	41;21542;21	21548			-0.02513	13	2294000000	1799600000
1919700000			6904	263	7098	18;14519;14	21554;21555	21557			0.004178	11	3613300000	3535100000
426230000			7085	263	7284	14898;14899	22183;22184	22174			-0.0075	38	850580000	784900000
28152000			7086	263	7285	10;14911;14	406;22207;22	22203			0.027685	9	3501400	51841000
1065500000			7087	263	7286	14914;14915	13;22214;22	22213			0.01545	5	4974700	1962000000
24807000			7180	263	7382	15104;15105	22514;22515	22513			-0.0165	4	52872000	45682000
0			7181	263	7383	15106;15107	22517;22518	22517			0.012805	1	89255000	0
1404300000			7183	263	7385;7386	63;15164;15	504;22605;2	22535	73		-0.0152	237	1465200000	2585900000
98654000			7386	263	7597	81;15682;15	69;23470;23	23471			0.104384	2	0	181670000
862300000			7713	263	7931	88;16389;16	539;24540;2	24457			0.157032	196	751540000	1587900000
140580000			7980	263	8203;8204	20;17021;17	93;25494;25	25494	74		0.022389	5	254220000	258880000
978370000			7981	263	8205;8206	17026;17027	00;25501;25	25501	74		0.058429	6	1475200000	1801700000
22649000			8047	263	8275	17185;17186	09;25710;25	25717			0.075389	99	30845000	41708000

Intensity membrane_low MW	Reverse	Potential contaminant	id	Protein group IDs	Mod. peptide IDs	Evidence IDs	MS/MS IDs	Best MS/MS	Oxidation (M) site IDs	Taxonomy IDs	Mass deficit	MS/MS Count	LFQ intensity membrane_high MW	LFQ intensity membrane_low MW
22307000			360	226	366	742;743	990;1091;10	1091			0.021595	3	0	41077000
164650000			885	226	909	;1895;1896;	;2851;2852;	2848			0.03526	8	406310000	303200000
1645700000			886	226	910	901;1902;19	;2864;2865;	2865			0.000548	18	5439700000	3030500000
55381000			896	226	920	;1924;1925;	;2900;2901;	2900			-0.25413	6	122530000	101980000
1381600000			897	226	921	;1929;1930;	908;2909;29	2908			-0.34913	11	1127000000	2544300000
294900000			898	226	922	;1934;1935;	;2916;2917;	2918			-0.31309	4	216080000	543050000
1730400000			921	226	945	;1992;1993;	007;3008;30	3002			-0.27885	15	1964400000	3186500000
172370000			922	226	946	996;1997;19	016;3017;30	3017			-0.29175	3	43577000	317410000
2142500			982	226	1009	2128;2129	3211;3212	3211			-0.17217	2	0	3945400
181580000			1000	226	1028	157;2158;21	258;3259;32	3261			-0.13272	7	458240000	334380000
29750000			1001	226	1029	;2161;2162;	;3266;3267;	3266			-0.09668	8	78356000	54784000
41039000			1094	226	1124	2334;2335	530;3531;35	3532			-0.10747	5	36621000	75573000
1195400000			1120	226	1151	;2382;2383;	604;3605;36	3603			0.014795	11	3995500	2201300000
15122000			1129	226	1160	;2403;2404;	643;3644;36	3642			0.037016	4	115720000	27848000
3120700			1130	226	1161	2406	3647	3647			0.043517	1	0	5746600
252370000			1323	226	1357	;2766;2767;	;4142;4143;	4139			-0.07243	8	579680000	464730000
2062900			1387	226	1422	2888	318;4319;43	4320			-0.12949	3	0	3798800
209040000			1479	226	1515	3055;3056	4529;4530	4529			-0.01237	2	744070000	384940000
440380000			1480	226	1516	3057;3058	532;4533;45	4533			-0.01594	5	601730000	810950000
2686800000			1552	226	1590	;3204;3205;	759;4760;47	4759			-0.2083	9	1285600000	4947600000
126700000			1674	226	1714	;3420;3421;	;5069;5070;	5072			0.001399	6	262740000	233320000
858480000			1829	226	1871	695;3696;36	;5456;5457;	5458			-0.08031	14	2047000000	1580900000
27483000			1830	226	1872	;3701;3702;	166;5467;54	5467			-0.10565	7	35988000	50610000
10294000			2177	226	2228	4411;4412	6569;6570	6569			-0.10975	1	34382000	18955000
11794000			2178	226	2229	4413;4414	571;6572;65	6571			-0.08633	3	43649000	21719000
1284900000			2243	226	2294	;4554;4555;	;6792;6793;	6792			-0.19541	4	2008800000	2366100000
192230000			2567	226	2621	;5296;5297;	;7895;7896;	7895			-0.02193	6	8648700	353990000
1395000000			2681	226	2738;2739	511;5512;55	230;8231;82	8206	43		-0.11983	51	1522600000	2568900000
296400000			2923	226	2988	007;6008;60	967;8968;89	8965			0.074515	9	469330000	545820000
318930000			2924	226	2989	013;6014;60	;8977;8978;	8979			0.091094	8	715750000	587310000
253120000			2925	226	2990	018;6019;60	;8986;8987;	8987			0.127134	8	586100000	466130000
204920000			3092	226	3159	410;6411;64	546;9547;95	9599			0.028133	300	190470000	377350000
1898100000			3094	226	61;3162;31	499;6500;65	;9776;9777;	9786	44;45		-0.01097	54	664950000	3495300000
2231000000			3117	226	3186	658;6559;65	;9886;9887;	9895			0.073969	20	2599500000	4108300000
2742000000			3446	226	3518	;7198;7199;	82;10783;10	10787			-0.13759	11	1149100000	5049300000
247470000			3656	226	3734	;7739;7740;	11640;11641	11638			-0.04427	5	152560000	455710000
289090000			3925	226	13;4014;40	361;8362;83	12561;12562	12574	46;47		-0.07879	32	1796300000	532360000
3782700			3926	226	4016	8369	12578	12578			-0.01904	1	0	6965800
750940000			5215	226	5375	99;11100;11	16576;16577	16573			0.023669	7	1596000000	1382800000
34401000			5228	226	5388	19;11120;11	04;16605;16	16607			-0.13434	5	6848000	63349000
197470000			5438	226	5603;5604	11564;1156	259;17260;1	17193	48		-0.08769	230	2138800000	363640000
319990000			5439	226	5605;5606	23;11624;11	17415;17416	17418	48		-0.03739	7	34771000	589250000
0			5584	226	5752	11902	21;17822;17	17822			0.020299	3	2379000	0
2413700			5862	226	6033	12414	22;18523;18	18522	49;50		-0.04907	3	0	4444800
0			5863	226	6034	12415	18525;18526	18526			0.003448	2	1505500	0
592880000			6349	226	6528	13373;1337	485;19886;19	19885			0.087315	7	1501500000	1091800000
72959000			6350	226	6529	77;13378;13	94;19895;19	19898			-0.00446	11	55625000	134350000
856370000			6895	226	7088;7089	88;14489;14	401;21502;21	21511	51		-0.11671	32	844090000	1577000000
2375200000			7246	226	7452;7453	62;15363;15	886;22987;22	22992	52		-0.03757	18	2039400000	4373900000
27214000			7247	226	7454	15368;1536	997;22998;22	22997			0.074669	3	0	50114000
13715000			7248	226	7455	15370	23000	23000			0.091247	1	0	25255000
279090000			7678	226	7895	74;16275;16	24335;24336	24331			0.045965	9	289200000	513930000
315010000			7679	226	7896	80;16281;16	48;24349;24	24342			0.061755	17	2921300000	580080000
0			8075	226	8303	17276	25842;25843	25842			-0.01888	2	4867300	0
368880000			8076	226	8304	17278;17279	46;25847;25	25846			0.006469	7	364160000	679290000
18813000			8077	226	8305	17282;17283	25853;25854	25851			0.002899	6	254730000	34644000
1815900000			8188	226	8419	17502;1750	56;26157;26	26153			-0.2021	11	2838100000	3344000000
108160000			8193	226	8424	17510;1751	72;26173;26	26169			-0.03964	8	584280000	199180000
304680000			8194	226	8425	17515;17516	26184;26185	26187			0.011674	14	1191100000	561070000